Date September 21, 2025
Contact person A. Hegazy
Telephone +31 (0)15 27 89201
E-mail A.R.Hegazy@tudelft.nl
Subject Response to Reviewers

Delft University of Technology

Delft Center for Systems and Control

Address
Mekelweg 2
2628 CD Delft
The Netherlands

www.dcsc.tudelft.nl

Anonymous Reviewer #1
Anonymous Reviewer #2
Anonymous Reviewer #3
Reviewers, Wind Energy Science

Dear Reviewers,

We sincerely thank you for your valuable and constructive feedback on our paper. Your comments have greatly assisted us in enhancing the quality of our work. We have carefully considered all of the points raised and revised the paper accordingly. This letter serves to address your comments and provide an overview of the changes made. Below, we will respond to each of your review comments, and at the end of this document, a colour-coded revised version is included showing the changes made to the manuscript.

Yours sincerely,

Amr Hegazy
Peter Naaijen
Jan-Willem van Wingerden

Enclosure(s): Response to comments of Reviewer #1
Response to comments of Reviewer #2
Response to comments of Reviewer #3
Colour-coded revised version

Response to comments of Reviewer #1

General comments:

- Referring to your comment about the writing style. This paper was not the result of a work that was written all around the same time. The first half of the paper is much older than as it was written at the beginning of my PhD, while the second part took place at the end of my PhD. All of this was compiled together to get this paper at the end.
- Regarding the gains used, a table with the employed gains was added to the SIMO controller section.

Specific comments:

Reviewer: Abstract: "feedback control": Specify the type, e.g., generator speed or power control.

Authors: *Thank you for noticing this. We have modified the text as follows:*
Text excerpt: "generator speed feedback control"

Reviewer: Abstract: "applying the same ... unstable": Clarify that only the pitch-to-feather scheme typically induces instability; other feedback control strategies exist that maintain stability in floating wind turbines.

Authors: *Thank you for your comment. The text was modified as follows:*
Text excerpt: "via the pitch controller to feather the blades, is well-established, employing the same controller gains with floating offshore wind turbines causes the turbines to become unstable."

Reviewer: Abstract: "fore-aft motion": Specify this is the nacelle fore-aft motion.

Authors: *Thank you for your comment. The text was modified as follows:*
Text excerpt: "the nacelle fore-aft motion."

Reviewer: Abstract: "more robust": Define what is meant by "robustness". Robust to what (e.g., model uncertainties, disturbances)?

Authors: *Thank you for your comment. This is explained in the following sentence in the text.*
Text excerpt: "which makes controllers often sensitive to unmodelled dynamics."

Reviewer: Lines 18–19: Remove "this is not ... know that" and "no wonder ... wind energy". These are unnecessary and informal.

Authors: *Thank you for your comment. The whole paragraph was modified as follows:*
Text excerpt: "Wind energy is essential to meeting the decarbonisation objectives of the European Union (EU) energy system, as it ensures delivering clean, affordable and secure electricity to various sectors, including households, industry and transport. Consequently, wind energy is expected to heavily contribute to the EU renewable energy targets, with wind energy already covering 19% of the EU's electricity demand in 2024. This has seen the EU revising the renewable energy directive, which lays down a minimum target of 42.5% share of renewables by 2030 with an aspiration to reach 45%. This is 10.5% higher than the initial 32% target. Subsequently, the EU could fulfil its ambition of becoming climate-neutral by 2050 [1]."

Reviewer: Lines 20–26: Consider whether this section is necessary. Is the article relevance limited to the EU context?

Authors: *Thank you for your question. While the article's relevance is indeed not limited to the EU context, the EU was the funding body as mentioned in the acknowledgements. However, a phrase was added to account for other continents as follows:*
Text excerpt: "As for the other continents, similar trends are observed [2]."

Reviewer: Lines 37–38: The phrase "while modifications ... to reducing the LCOE" is vague. Co-design of turbine and platform may reduce LCOE. Please clarify the mechanism you're referring to.

Authors: *Thank you for your comment. Since it is not clear to the reader, we clarified this by modifying the text as follows:*
Text excerpt: "Developing new control architectures can contribute to reducing the LCOE. Another approach is control co-design [3], which has proven to be highly effective."

Reviewer: Line 80 and following: Including physical units is not necessary. Models can use different units.

Authors: *Thank you for your comment. While this is definitely correct, to our understanding, including the units is part of the journal's submission requirements. Furthermore, it helps with reproducing the results of the paper.*

Reviewer: Line 87: "and a non-linear function f(x) = 0". Unclear connection with the surrounding text.

Authors: *Thank you for your comment. The whole paragraph was modified as follows:*
Text excerpt: "with ρ (kg.m^{-3}) as the air density, R (m) being the rotor radius, $C_p(\lambda, \beta)$ as the power coefficient, which depends on the blade pitch angle, β (rad), and the tip-speed ratio, $\lambda = \Omega R/vN_{gb}$, with v (m.s^{-1}) being the wind speed normal to the rotor plane. At steady-state, the non-linear wind turbine dynamics in Eq.(1) can be linearised using first-order Taylor series expansion around an equilibrium point as:"

Reviewer: Line 98: Instead of "remains constant ... and assumption errors", state clearly that the control strategy assumes accurate knowledge of k_g.

Authors: *Thank you for your comment. The text was modified as follows:*
Text excerpt: "It is fair to mention that the controller in Eq.(4) assumes a constant k_g throughout the wind turbine's lifetime."

Reviewer: Line 113: "Notice that the terms irrelevant to the control problem". Please specify which terms are considered irrelevant and why.

Authors: *Thank you for your comment. The text was modified as follows:*
Text excerpt: "Equation (3) represents the closed-loop system of the wind turbine in the above-rated region. Therefore, only the terms containing ψ and its derivatives are considered [4]. The remaining terms are irrelevant to the control problem and therefore do not appear in Eq. (6)."

Reviewer: Line 131: The definition of above-rated operation is incorrect. Rated wind speed is the minimum at which rated power is produced. All higher wind speeds are above-rated.

Authors: *Thank you for your comment. The definition is actually meant for the steady state thrust in the above-rated region in particular.*

Reviewer: Line 133: "The steady-state ... generator speed variations". This appears inaccurate. In above-rated conditions, pitch is increased to limit aerodynamic torque. Clarify.

Authors: *Thank you for your comment. The text was modified as follows:*
Text excerpt: "The steady-state blade pitch angle varies along the operating curve to limit the aerodynamic torque and reduce the oscillation in the power production. The generator torque is kept constant instead of constant power since this strategy limits the generator speed variations, hence, reduces drive train loads and pitch activity [5]."

Reviewer: Line 135: "The objective is to achieve ... differential diminishes". Unclear. Please rephrase for clarity.

Authors: *Thank you for your comment. The sentence was removed since it did not fit in this paragraph.*

Reviewer: Line 138: "capturing the critical dynamics". Specify what these critical dynamics are. Are you referring to adding platform pitch to drivetrain dynamics? State clearly which degrees of freedom are included and which are not, along with your rationale.

Authors: *Thank you for your comment. The text has been modified as follows:*
Text excerpt: "To form a FOWT mathematical model, the generic 1-DOF model of the wind turbine in Eq. (3) is combined with the floating platform dynamics. For the sake of explaining the negative damping problem analytically, only a 2-DOF FOWT model capturing the critical dynamics is used, where the platform pitch degree of freedom (DOF) is primarily considered to characterise platform dynamics, as the negative damping instability is most pronounced at the platform pitch eigenfrequency, where there is no damping from the mooring and vary little hydrodynamic damping leading to negative damping if the pitch control is fast [5, 6]."

Reviewer: Line 149: "omitting radiation damping ... frequency-dependent coefficients". This choice is questionable. Why are some terms relevant only in certain scenarios? Clarify.

Authors: *Thank you for your comment. For a spar platform, the radiation damping is relatively small compared to the viscous damping. It is almost equal to zero across all frequencies except around the natural frequency of the mode of interest. Regarding the added mass, it can be assumed constant across all frequencies, which is pretty much the case. Therefore, computing the added mass using Morison's equation is valid. For a semi-sub (triple spar), the same assumption applies, whereas for other platforms with different geometries, it might not be the case. The references .[7, 8] explain the reason for the omission.*

Reviewer: Line 181: "clearly shows ... via the term". Why is this term important?

Authors: *Thank you for your comment. The whole sentence was removed as its importance emerges later in section 3.3 where it is discussed.*

Reviewer: Line 192: "is of the main interest". Justify why this is the main interest.

Authors: *Thank you for your comment. The text was modified as follows:*
Text excerpt: "For the feedback control of FOWTs in Region 3, the control objective is to reduce the generator speed oscillations using the blade pitch action. Consequently, the TF, $G_{\Omega,\beta}$, mapping the blade pitch angle to the generator speed, in Eq. (16) is of the main interest:"

Reviewer: Line 205: "quasi-static ... wind speed". Define quasi-static equilibrium more precisely. What does it mean that system variables are "balanced"?

Authors: *Thank you for your comment. The text was modified as follows:*
Text excerpt: "In a closed-loop FOWT system at steady state, the gradient dF_a/dv is positive below-rated wind speed, meaning the thrust force increases as wind speed rises."

Reviewer: Line 208: "modifies the force direction". Unclear. What force? How is the direction modified?

Authors: *Thank you for your comment. The part was removed as it was incorrect.*

Reviewer: Line 229: "the pitch angle ... are negative". I think you are mixing gradients and steady state values. The derivatives of thrust and aerodynamic torque w.r.t. blade pitch are negative. As the wind speed increases, the blade pitch is drecreased to have constant aerodynamic torque (hence to balance the increase it would have because of wind speed). The increase in blade pitch doesn't yield constant thrust but thrust decreases.

Authors: *Thank you for your comment. We agree with the thrust and aerodynamic gradients being negative wrt blade pitch. However, we beg to differ with the rest of the sentence, as when the wind speed increases, the blade pitch increases too to keep the balance between the aerodynamic and generator torques, and avoid accelerating the rotor. The aerodynamic torque decreases too in the process.*

Reviewer: Line 293: "this approach". Please clarify which approach is being referred to.

Authors: *Thank you for your comment. The text was modified as follows:*
Text excerpt: "Applying the global detuning approach."

Reviewer: Line 299: The explanation regarding gain tuning and stability is not clear. Rephrase.

Authors: *Thank you for your comment. The text was modified as follows:*
Text excerpt: "Rather than applying a global detuning strategy at all the operating points as described in the previous section, a more effective method involves individually tuning the PI controller for the fastest achievable response at each operating point, while still ensuring the stability of the linear system [9, 10, 11, 12]. However, achieving a stable system is not sufficient in control design; the system must also exhibit adequate stability margins, which indicate how close it is to instability and how robust it is to disturbances."

Reviewer: Line 313: "a range of ... ζ_c". Define these parameters explicitly.

Authors: *Thank you for your comment. The text was modified as follows:*
Text excerpt: "a range of the Proportional-Integral (PI) control parameters, namely, the natural frequency (ω_c) and the damping ratio (ζ_c)"

Reviewer: Line 321: The effects of ω_c and ζ_c on bandwidth and stability are difficult to interpret without definitions. Please clarify.

Authors: *Thank you for your comment. They were defined as per your comment above. They were also introduced and defined in section 2 in the equations from 6 to 8.*

Reviewer: Line 326: What is ω_p and how does it differ from ω_c? Define all parameters clearly.

Authors: *Thank you for pointing this one out. There was a typo and it should have been* ω_c.

Reviewer: Line 336: "regularisation terms". Briefly explain what regularization is used for in this context.

Authors: *Thank you for your comment. The text was modified as follows:*
Text excerpt: "Regularisation terms may be added to the objective function to fulfil control objectives such as minimising the generator speed and power oscillations, as well as reducing the loads [9], and limiting the control gains [12]."

Reviewer: Lines 371, 377: "blade pitch damping" ???

Authors: *Thank you for your comment. The title was changed to "additional blade pitch loop".*

Reviewer: Line 400: "should this objective ... it will be unstable". Unclear. Explain what the objective is and why instability would result.

Authors: *Thank you for your comment. The text was modified as follows:".*
Text excerpt: "Should the objective of decoupling the drivetrain and the platform dynamics be sought, extra filtering is required to change its dynamics; otherwise, the system damping worsens and it becomes unstable."

Reviewer: Line 463: "It was learnt ... band-pass filter". Why is it feasible to retain the PI controller and what is the role of the band-pass filter?

Authors: *Thank you for your comment. As mentioned in the text, those control structures for the blade pitch and the generator torque, were obtained based on*

$$\mathcal{H}_\infty$$

optimisation as explained in [13]. First, the structure of the different control loops was learnt via $\mathcal{H}_\infty$ synthesis. For the blade pitch the returened structure was more of a low-pass filter, while a band-pass filter for the generator torque. Afterwards, the structure of both was fixed to basic control elements, ensuring the same performance. Therefore, the blade pitch loop retained the PI structure, and the generator torque became an inverted-notch filter. We strongly, advise you to refer to this publication [13]. The text was also modified as follows:

Text excerpt: "It was learnt from $\mathcal{H}_\infty$ control synthesis that the blade pitch maintains the PI structure, while the generator torque requires an inverted-notch filter hegazy2023. From its name, an inverted-notch filter is a control element that is only operational at a specific frequency. Thinking about it, such a control structure, resulting from the $\mathcal{H}_\infty$ synthesis, for the generator torque control loop is reasonable since the generator torque input should not operate across all frequencies, but only around the RHPZs frequency where the blade pitch input is blocked. Therefore, the generator torque control loop takes over."

Reviewer: Line 468: "an inverted notch". Clarify the purpose of using an inverted notch filter.

Authors: *Thank you for your comment. This was explained in the previous comment and the text was modified accordingly.*

Reviewer: Line 519: "to compensate for ... aerodynamic damping". Rephrase for clarity. What is being compensated, and how?

Authors: *Thank you for your comment. The text was modified as follows:*

Text excerpt: "its main objective is to add damping to the closed-loop system, through extra blade pitch action, to compensate for the severe reduction in the overall system damping caused by the negative aerodynamic damping"

Technical corrections:

Reviewer: Line 42: Remove "peak to peak".

Authors: *This part has been removed as advised.*

Reviewer: Line 80: Remove "(kg.m2)" and similar notations. The dot is not conventionally used.

Authors: *The dot was removed from the units as advised.*

Reviewer: Line 121: Replace "lie in the vicinity of" with "include".

Authors: *The text was modified as advised.*

Reviewer: Line 272: Remove "a point that is elaborated further in this section". It's redundant.

Authors: *The text was removed as advised.*

Reviewer: Line 277: Replace "triggered by" with "associated with"; replace "causing" with "causes".

Authors: *The text was modified as advised.*

Reviewer: Line 320: Consider replacing "failure" with "instability" if that's what you meant.

Authors: *The text was modified as advised.*

Reviewer: Line 325: Replace ":" with ",".

Authors: *The text was modified as advised.*

Reviewer: Lines 367–368: Replace "actuators" with "actuation".

Authors: *The text was modified as advised.*

Reviewer: Figure 15: Adjust the line style for to improve readability.

Authors: *Line style has been adjusted as advised.*

Reviewer: Figure 15 caption: Explain which transfer function the Bode plot represents.

Authors: *Caption has been modified for further explanation as follows:*
Text excerpt: "Bode plot of the normalised MISO plant $\bar{G}$ illustrating the frequency response of each control channel separately (solid lines) as well as the response of the SISO plant $\tilde{G}$ in case of the linear combination of both actuators (dashed line) where the blade pitch actuator is active till a certain frequency before its authority deteriorates, thus, the generator torque actuator takes over from that frequency onwards."

Reviewer: Figure 16, magnitude: I think one dot is missing. Figure 16, phase: one vertical line is hard to see.

Authors: *Thank you for your comment. At first glance, it seems that the dot corresponding to the gain margin is missing for the artificial SISO plant ($\hat{G}$). However, it is not the case since for this linear transfer function, at a certain operating point, and after the modifications that have been applied, the gain margin is infinite. Regarding the phase, the vertical line illustrating the phase margin is hard to see since it is actually very small, which indicates less controller robustness.*

Reviewer: Line 510: Replace "how impressive of a difference" with "the significant impact".

Authors: *The text was modified as advised.*

Reviewer: Line 531: Remove repeated citation. Only cite once unless needed.

Authors: *Repeated citations were removed as advised.*

Reviewer: Figure 17: Reduce line thickness to avoid covering differences.

Authors: *Those lines were removed as per your suggestion and considered before Table 3.*

Reviewer: Line 547: Replace "dramatic" with "large".

Authors: *The text was modified as advised.*

Response to comments of Reviewer #2

General comments

Reviewer: Clarify the turbine model used (which platform, rating, etc.).

Authors: *Thank you for noticing this. The text was modified to include this important piece of information in section 2.1 and again in the results section.*

Reviewer: Clarify the site conditions assumed, i.e. wave height, period, wind shear, TI.

Authors: *Thank you for your comment and advice. The text was modified to clarify this in the results section.*

Reviewer: Clarify the controller architecture and changes of existing controllers from the literature.

Authors: *Thank you for your comment. All the control architectures are explained analytically and graphically, as illustrated by the figures and equations corresponding to each controller.*

Reviewer: Tabulate used controller gains for reproducibility of results.

Authors: *Thank you for your comment and advice. A table with all the gains was added as advised.*

Reviewer: Clarify structure of new SIMO controller, especially why the plant is changed. I expected only K to change, not the plant.

Authors: *Thank you for your comment. The modification applied to the plant primarily aimed to bring the loop gain of both input channels to unity, ensuring they have comparable gains and that their optimisation-based tuning could be properly performed.*

Reviewer: Discuss sensitivity to sea state: Often controllers perform well in benign sea states but fail in harsher conditions. It should be proven that the controllers don't amplify first-order wave motions.

Authors: *Thank you for your comment. The sea state was defined in the results section as previously advised, where a challenging sea state was used in the simulations. Apart from that, the controller is actually blind to the first-order wave effects as they do not appear in the response since they operate at higher frequencies than the controller's natural frequency, while the low-frequency dynamics are of interest. We refer you to [14] where this subject was explained through wave tank experiments.*

Reviewer: Improve comparability of the results: Some controllers use a lot of generator torque actuation, while others don't.

Authors: *Thank you for your comment. This has to do with the tuning and also to showcase that the SIMO controller can better reduce rotor speed oscillations at the expense of more generator torque actuation.*

Specific comments

Reviewer: Line 38: "should not be overlooked as it can significantly contribute to reducing the LCOE." How?

Authors: *Thank you for your question. The text was modified as follows:*
Text excerpt:"Developing new control architectures can contribute to reducing the LCOE. Another approach is control co-design [3], which has proven to be highly effective."

Reviewer: Line 56: "control channels are separately tuned to achieve improved dynamic responses of a specific output." Clarify what this means exactly. What is a "control channel"? Is compartmentalised the same as "segmented" control? How does it relate to the "multi-SISO" approach (see Fleming2016) and the terms "sequential", or "decentralised" control?

Authors: *Thank you for your comment. The text was modified for clarification as follows:*
Text excerpt:"Systems with more than one actuating control input and more than one sensor output may be considered as multivariable systems or Multi-Input-Multi-Output (MIMO) systems. The control objective for multivariable systems is to obtain a desirable behaviour of several output variables by simultaneously manipulating several input channels. A FOWT is a MIMO system. To evaluate such a system, MIMO transfer function matrix is needed. In many FOWT control strategies, the feedback control loops are often designed separately in a decoupled format, with each control loop tuned to improve the response of a specific output [15]. This means that the multivariable controller design is reduced to a series of single-loop controllers. Although this approach is common, the loops in a MIMO system are dynamically coupled. As a result, changing the settings of one control loop can affect the behaviour of other loops, causing interaction between them. Subsequently, the interaction between the different control loops of a system should be dealt with simultaneously."

Reviewer: Line 65: tutorial or a review?

Authors: *Thank you for your question. It was changed to "review" instead.*

Reviewer: Line 105: introduce Ω_{rat}.

Authors: *Thank you for noticing this. The text was modified as follows:*
Text excerpt:"At above-rated wind speeds (referred to as Region 3), a conventional wind turbine controller relies on the blade pitch to regulate the generator speed to its rated value, Ω_{rat}."

Reviewer: Equation 6: Clarify if the generator torque is constant.

Authors: *Thank you for your comment. This is mentioned in the paragraph above Eq. 6.*

Reviewer: Line 113: does this mean that changes in relative wind speed are irrelevant? How can you then model negative damping?

Authors: *Thank you for your comment. The changes in the relative wind speed are included in Eq. 13 due to the rigid body motion of the floater.*

Reviewer: Line 150: clarify which types of models you're using. What is the "control model", as opposed to the "simplified 2D model"

Authors: *Thank you for your comment. The text was modified as follows:*
Text excerpt:"However, to preserve key dynamic couplings, the control model used for the control design must include additional modes that capture the most significant system dynamics, namely the platform's surge and heave, and the tower first fore-aft bending [9]; otherwise, some interactions within the system may be overlooked [10]."

Reviewer: Equation 11: How about surge motion?

Authors: *Thank you for your comment. The surge motion is not as problematic as the pitch since the negative damping instability arises due to the pitch motion. The system zeros corresponding to the surge motion always lie in the left half plane. This we already showed in [13]. So for the sake of the analytical model, we excluded the surge motion in the simplified 2D model. However, in the control model used for the synthesis, the surge motion was included.*

Reviewer: Line 206: "gradient dF_a/dv is positive below-rated wind speed" Clarify if you're referring to an OL or CL system.

Authors: *Thank you for you comment. The text was modified as follows:*
Text excerpt:"In a closed loop FOWT system at steady state, the gradient dFa/dv is positive below-rated wind speed" Clarify if you're referring to an OL or CL system."

Reviewer: Line 209: "As a consequence, aerodynamic damping is positive at below-rated wind speeds but turns negative at above-rated wind speeds." Note that this is only true in CL.

Authors: *Thank you for your comment. This was clarified in the previous comment.*

Reviewer: Equation 22: Why is there the torque in the equation of the thrust?

Authors: *Thank you for your comment. From Eq. 19, where Ω_r is constant, an expression was obtained for the blade pitch differential in Eq. 20. Plugging Eq. 20 into Eq. 21, reach such an expression in Eq. 22, which is also derived in Eq. 18.*

Reviewer: Line 249: "A zero represents a critical frequency, referred to as the frequency of the zero" This sentence is unclear.

Authors: *Thank you for noticing this. The text was modified as follows:*
Text excerpt:"The roots of the numerator of a transfer function are called zeros (denoted by ◯ in Fig. 3)."

Reviewer: Line 293: "bandwidth" The bandwidth is only constant if the platform pitch natural frequency does not change across operating points.

Authors: *Thank you for your comment. The platform pitch natural frequency is a system property and does not change across the operating points. The detuning process initially was applied such that the bandwidth stays constant [16, 17] across all the operating points, such that its value does not exceed the platform pitch natural frequency.*

Reviewer: Line 354: "The optimisation goal is to minimise" repetition.

Authors: *This part was removed as advised.*

Reviewer: Line 46: Doesn't this mean that rotor speed changes resulting from free-stream wind have the same effect?.

Authors: *Thank you for your question. The main point of developing this controller is to prove that the parallel compensation can still be applied without the platform pitch motion sensor. The rotor speed response to the wind disturbance changes since the controller has a different structure from the other controllers presented before, which can be seen in the results section. If we are looking at the frequency response from the wind disturbance to the rotor speed in a Bode plot, there will be no change since the controller was synthesised to have generator speed error as input and a combination of blade pitch and generator torque output. However, the relative wind speed effect, due to the platform pitch motion in particular, is the one that is going into the controller, and being reduced.*

Reviewer: Line 468: Above, you say that the platform pitch measurement is not needed, which is the measurement going into this controller?

Authors: *Thank you for your question. Indeed for the SIMO controller, the platform pitch measurement is not needed, as it only rely on the generator speed measurement as illustrated in Fig. 13.*

Reviewer: Figure 14: What does $\bar{G}(s)$ stand for?.

Authors: *Thank you for noticing this one. It has been defined in the text now. It stands for the normalised plant. The text was modified as follows:*
Text excerpt:"In order to do that, the original MISO plant $G(s)$ is normalised to $\bar{G}$ such that the magnitude of both the blade pitch and the generator torque input channels becomes unity so that both control inputs are of comparable effect."

Reviewer: Line 504: Which is the FOWT design used, rated power, what is the wave height?.

Authors: *Thank you for noticing that. The FOWT design used has been introduced earlier in the text and added also here together with the environmental conditions. The text was modified as follows:*
Text excerpt:"The FOWT system (NREL 5-MW RWT jonkman2009definition atop OC3 floater jonkman2010definition) was simulated in OpenFAST Openfast with the five controllers discussed in Section ?? in environmental conditions of turbulent wind and irregular waves. The simulations were conducted in the above-rated Region 3 ($v_{rated} = 11.4$ m/s) at average wind speeds ranging from 12 m/s to 24 m/s, with TurbSim TurbSim to simulate the turbulent wind field, where the International Electrotechnical Commission (IEC) Kaimal spectral model was used as a turbulence model with a turbulence intensity of 14%. The irregular waves were generated using JONSWAP spectrum at a significant wave height $H_s = 3$ m and peak period $T_p = 12$ s."

Reviewer: Figure 17: The first-order wave response is not visible here. Are waves enabled in the simulation?

Authors: *Thank you for your question. The first-order wave effects do not appear in the response as they operate at higher frequencies than the controller's natural frequency, and thus the controller do not react to the incoming waves although they are enabled in the simulation.*

Reviewer: Line 605: Why does the SIMO controller saturate, but the others don't (i.e. they use smaller gains which prevent saturation). Wouldn't it make sense to use the same strategy for all?.

Authors: *Thank you for your question. If we look at the relative gain array of plant at zero frequency for above rated wind speeds, or in other words compare the loop gain of the transfer function mapping the generator torque to the generator speed (G_{Ω,τ_g}) to that of the one mapping the blade pitch to the generator speed ($G_{\Omega,\beta}$), we will find that the loop gain of $G_{\Omega,\beta}$ is significantly larger than the one of G_{Ω,τ_g} indicating that G_{Ω,τ_g} requires much higher gains at above rated conditions to be able to do something. Maybe a some reduction in the gain might prevent saturation, but that indeed this is the challenge facing this controller.*

Response to comments of Reviewer #3

When we first started writing this paper, it was not the plan to include the sections before section 3.3.3 (the key section, as you call it). However, as the writing progressed, we thought of adding sections 3.1, 3.3.1 and 3.3.2. But we thought that it would be nice to compare the new controller against the existing controllers out there addressing the same control problem. Whereas, section 3.2 was a late addition, and we thought that it would make the comparison a bit more complete, although it is not the case since there are a few still missing, mainly from the CSM MIMO paper as per your nomenclature, but we decided to stop at that point. Having decided to add those additional sections to draw a more complete picture, this is how this paper turned out to be.

Reviewer: The authors of WES-2025-68 refer to their paper as a tutorial, e.g. on page 3, line 65, they state "This paper provides a tutorial on the design of closed-loop controllers for FOWTs . . . " and indeed they go into some detail in reviewing the various controllers. Given that they cite a different paper in the same special IEEE CSM issue, it is surprising that they don't cite the main tutorial paper in this CSM special issue. It would be useful for the authors of WES-2025-68 to explain why they believe another (very similar) tutorial paper is needed so soon after the 30-page October 2024 tutorial paper in the IEEE CSM.

Authors: *Thanks for your comment. When developing new controllers, there must be references to compare the performance of the new controllers against. That is why we included those previously proposed controllers. Having said that, we cite the ACC paper and this paper has considerable similarities with the CSM tutorial paper*

Reviewer: Figure 1 of WES-2025-68 looks quite similar (even in style) with Figure 3 of the CSM MIMO paper. Of course, I do expect that authors may have similar wind turbine diagrams; and I only noted this particular similarity after having marked many of the other similarities enumerated below.

Authors: *Thank you for your comment. Looking at Figure 3 of the CSM MIMO paper in depth, we are 100% that different tools were used to generate both figures. They might seem similar at first glance, but the similarity is not clear.*

Reviewer: Figure 3 of WES-2025-68 is quite similar to Figure 2 of the main CSM tutorial paper. The numerical values are not exactly the same, as the floating wind turbines considered are different in the two papers.

Authors: *Thanks for you comment. We have the same figure in our IFAC paper, which was published before the CSM tutorial paper, and in the field, it is really common to use those kinds of figures. The difference in this paper is that the system has a lower number of states, and we show only the upper half of the figure. Anyway, we have modified the figure to show the upper and lower half planes.*

Reviewer: The particular architectures reviewed in WES-2025-68, as illustrated in its Figures 4, 9, and 11, are special cases of Figure 2 in the CSM MIMO paper and are also separately discussed in the CSM MIMO paper. A summary discussion is also provided in the main CSM tutorial paper (e.g. Figure S12).

Authors: *Thanks for your comment. The particular architectures in Figures 4, 9 and 11 were in our IFAC paper, which was published before the two papers being referred to.*

Reviewer: Lines 54 to 59 of Page 2 in WES-2025-68 read: "A multi-loop feedback system evaluation requires a Multi-Input, Multi-Output (MIMO) transfer function representation. Those multi-loop FOWT control strategies in the literature often employ a compartmentalised feedback design, where individual control channels are separately tuned to achieve improved dynamic responses of a specific output. While this segmented tuning methodology remains widespread, inter-loop dynamic coupling inherent in MIMO architectures generates cross-channel interference phenomena, whereby localised parameter adjustment in a single control loop perturbs the closed-loop response characteristics of adjacent feedback channels." A similar paragraph in the right-hand column on page 64 (in the special issue) of the previously published 2024 CSM MIMO paper reads: "Many multiloop FOWT control design approaches in the literature use single-loop closure, where each loop is designed in isolation with simplifying assumptions, typically to target improvement of a single-output behavior. For example, the common constant-power control loop is designed to decrease the dependence of generator power variations on generator speed variations, but it also has the side effect of reducing the natural stability of the FOWT system. Tuning each loop in isolation is common practice, although coupling between multiple loops means that tuning of one loop most often induces changes in the behavior targeted by another, and a tradeoff is necessary to satisfy multiple performance objectives."

Authors: *Thank you for your comment. Both paragraphs give pretty much the same meaning, but they are not similar. Moreover, we already cited the CSM MIMO at the end of the paragraph. Furthermore, this is common knowledge that can be found in any textbook about multivariable control. Anyway, the paragraph was rephrased as follows:*

Text excerpt:"Systems with more than one actuating control input and more than one sensor output may be considered as multivariable systems or Multi-Input-Multi-Output (MIMO) systems. The control objective for multivariable systems is to obtain a desirable behaviour of several output variables by simultaneously manipulating several input channels. A FOWT is a MIMO system. To evaluate such a system, MIMO transfer function matrix is needed. In many FOWT control strategies, the feedback control loops are often designed separately in a decoupled format, with each control loop tuned to improve the response of a specific output. This means that the multivariable controller design is reduced to a series of single-loop controllers. Although this approach is common, the loops in a MIMO system are dynamically coupled. As a result, changing the settings of one control loop can affect the behaviour of other loops, causing interaction between them. Subsequently, the interaction between the different control loops of a system should be dealt with simultaneously."

Reviewer: Equation (14) of WES-2025-68 is the same as Equation (14) in the main CSM tutorial paper, except the orders of the states and inputs have been changed. Similarly, Table 1 in WES-2025-68 is the same as Table 1 in the main CSM tutorial paper, except with some different symbols and notation used. While control-oriented models may end up being of similar forms, it is quite uncanny how the presentation of the model in WES-2025-68 is also so similar to that in the previously published main CSM tutorial paper.

Authors: *Thank you for your comment. Table 1 was removed, and the model presentation is based on our IFAC paper except that we excluded the platform surge DOF.*

Reviewer: The discussion and analysis of the condition for non-minimum phase zeros on pages 9-12 of WES-2025-68 are similar to both the main CSM tutorial paper (pages 40-42 of the CSM special issue) and the CSM MIMO paper (page 67, which references the main CSM tutorial paper). All of these analyses are based on previous work, especially that of [18].

Authors: *Thank you for your comment. This discussion and analysis is also similar to our IFAC paper from 2023. The analyses are indeed based on the work of [18], and we stated that explicitly.*

Reviewer: The stability margin discussion on pages 14-16 of WES-2025-68 is very similar to the Robust Controller Tuning section in the CSM MIMO paper (page 69). In particular, the contour plots on page 15 of WES-2025-68 are very similar to those in Figures S1 and S2 in the CSM MIMO paper, again with different specific numerical results because different floating wind turbines are considered in these papers. The authors of WES-2025-68 have added an additional term in their cost function (Equation (24)) to directly address control effort (control saturation), while the authors of the CSM MIMO paper discuss "constraining or regularizing the controller gains in the tuning optimization" to mitigate controller saturation (page 75).

Authors: *Thank you for your comment. Somewhere in the text, a referral to the CSM MIMO paper was added, explaining that this specific section is built upon it. Consequently, the figures on page 15 are similar, while the one on page 16 is new, corresponding to the modification of the objective function. Regarding the regularisation, that was already acknowledged in the text, mentioning that the process was not clearly explained in the CSM MIMO paper when we tried to reproduce the results. That led to the modification of the cost function to constrain the controller gains explicitly.*

Reviewer: Section 3.3.1 in WES-2025-68 is very similar to the Blade-Pitch Platform Damping section of the CSM MIMO paper (pages 73-74 in the CSM special issue). Given the overlaps that I was noticing, I also looked up the Stockhouse et al., Wind Energy, 2024 paper4 (which I will refer to as the WE paper) and note that this Section 3.3.1 of WES-2025-68 has similar ideas as Section 3.1.2 in the WE paper. In particular, the idea of tuning the "strength" of k_β via a ξ_β parameter that varies from 0 to 1 already appeared in the WE paper with the α_β parameter in Equation (18) in the WE paper. While perhaps the authors of WES-2025-68 are meaning to review this MISO control structure from past papers, they do not cite either the CSM MIMO paper or the WE paper in Section 3.3.1 in WES-2025-68. They do cite (Jonkman, 2008; van der Veen et al., 2012) early in Section 3.3.1, but the tunable "strength" of k_β does not appear in either of these much earlier papers.

Authors: *Thank you for your comment. The idea of tuning the strength k_β via ξ_β also appeared in our IFAC paper in 2023. Anyway, a citation was added for the tunable strength.*

Reviewer: Similarly, Section 3.3.2 in WES-2025-68 is very similar to the Parallel Compensation section of the CSM MIMO paper (pages 74-75), including the tunable ξ_{τ_g} parameter (which is α_{comp} in the CSM MIMO paper and α_τ in the WE paper).

Authors: *Same as above.*

Reviewer: Lines 573-577 on page 30 of WES-2025-68 state: "Based on these findings, the authors recommend an adaptive approach, where different proposed controllers are alternated depending on environmental conditions and control objectives. For example, at certain times, the turbine operator may prioritise minimising generator speed oscillations and activate the corresponding controller. At other times, the focus may shift to reducing structural loading, necessitating a different control strategy. Since no single controller can simultaneously optimise all objectives—some of which may be conflicting—dynamic selection based on operational priorities is advised."
The conclusion of the CSM MIMO paper (page 79) states: "Four multiloop FOWT-control approaches have been analyzed and compared to a stable single-loop baseline controller. The simulation performance of these controllers shows the tradeoffs in designing a multiloop controller. Wind energy producers must balance instantaneous power-regulation demanded by grid operators while ensuring operational safety and component longevity for the lifetime of a wind farm. Multiloop control designs can schedule the usage and combination of multiple control loops at different points of the operating region to garner performance benefits, while mitigating drawbacks of each control strategy. The control approaches taken in this work are intended to serve as a basis for the intuitive understanding of the impact of structured multiloop control on FOWT system dynamics."

Authors: *Thank you for your comment. For a paper comparing different controllers, and for someone who has an interest in the control of floating wind turbines, you would know that you can not achieve everything with one single controller. Therefore, such a conclusion is normal to arrive at.*

Reviewer: Section 3.3.3 may be the key section that appears to be new in WES-2025-68, and is based on the authors' earlier 2023 IFAC World Congress paper. So a question is whether such a full-length paper is warranted for the contribution in Section 3.3.3, and perhaps the addition of a control effort term to the objective function used in the optimization.

Authors: *Thank you for your question. Based on the previous comments, it seems that the only part considered in the IFAC paper is section 3.3.3, although there are other sections, which are simply sections 3.1, 3.3.1, 3.3.2 that were totally neglected. Moreover, it is to our understanding that using your own previously published work is not against the journal's policy as long as it is built upon and extended, which we simply did here. Additionally, we need the other controllers to compare against, which was also done in the CSM MIMO paper.*

Reviewer: While I do realize that accessing the IEEE Control Systems Magazine requires a subscription or membership in the IEEE Control Systems Society, whereas the Wind Energy Science journal is an open-access journal, many major universities with multiple engineering departments have institutional subscriptions to IEEE Xplore that include the IEEE Control Systems Magazine. Further, many control systems researchers are indeed members of the IEEE Control Systems Society. A question is then: what are the rules for overlapping material and ideas with already-published papers, possibly in journals that require a subscription? Do the above similarities give others pause, or am I an outlier in finding this amount of overlap disturbing? My own opinion is that newly submitted manuscripts should not have substantial overlap with previously published papers, regardless of whether they are open-access or not.

Authors: *Thank you for this question. The two papers that you referred to were based on the papers published at the 2023 ACC as you mentioned below, which is not against the rules of IEEE. We also have had our paper published in 2023 in IFAC, and we are extending it while sticking to the rules of Wind Energy Science.*

Reviewer: I spent quite some time on this review, but really wanted to be as careful as possible in forming this opinion before writing all of this up. I found that the October 2024 IEEE CSM special issue is largely based on a special so-called "tutorial session" at the 2023 American Control Conference (ACC), and earlier versions of both the CSM MIMO and main CSM tutorial papers were published at the 2023 ACC (and also available via IEEE Xplore), so many of these ideas were already published in 2023.

Authors: *Thank you for your comment. Our IFAC paper was also published at the 2023 IFAC [13].*

References

[1] European Commission. European Wind Power Action Plan., 2023. (accessed: 16-11-2023).

[2] GWEC. Global wind report 2025. Technical report, Global Wind Energy Council, 2025.

[3] Lucy Y. Pao, Manuel Pusch, and Daniel S. Zalkind. Control co-design of wind turbines. *Annual Review of Control, Robotics, and Autonomous Systems*, 7(Volume 7, 2024):201–226, 2024.

[4] J. Jonkman, S. Butterfield, W. Musial, and G. Scott. Definition of a 5-MW reference wind turbine for offshore system development, 2009.

[5] T J Larsen and T D Hanson. A method to avoid negative damped low frequent tower vibrations for a floating, pitch controlled wind turbine. 75:012073, 2007.

[6] Jason Jonkman. Influence of control on the pitch damping of a floating wind turbine. In *46th AIAA Aerospace Sciences Meeting and Exhibit*. American Institute of Aeronautics and Astronautics, 2008.

[7] Frank Lemmer, David Schlipf, and Po Wen Cheng. Control design methods for floating wind turbines for optimal disturbance rejection. In *Journal of Physics: Conference Series*, volume 753, page 092006. IOP Publishing, 2016.

[8] Frank Lemmer, Wei Yu, Birger Luhmann, David Schlipf, and Po Wen Cheng. Multibody modeling for concept-level floating offshore wind turbine design. *Multibody System Dynamics*, 49(2):203–236, 2020.

[9] Frank Lemmer, Wei Yu, David Schlipf, and Po Wen Cheng. Robust gain scheduling baseline controller for floating offshore wind turbines. 23(1):17–30, 2020.

[10] Wei Yu, Frank Lemmer, David Schlipf, and Po Wen Cheng. Loop shaping based robust control for floating offshore wind turbines. In *Journal of Physics: Conference Series*, volume 1618, page 022066. IOP Publishing, 2020.

[11] David Stockhouse, Manuel Pusch, Rick Damiani, Senu Sirnivas, and Lucy Pao. Robust multi-loop control of a floating wind turbine. *Wind Energy*, 27(11):1205–1228, 2024.

[12] David Stockhouse and Lucy Y. Pao. Multiloop control of floating wind turbines: Tradeoffs in performance and stability. *IEEE Control Systems*, 44(5):63–80, 2024.

[13] Amr Hegazy, Peter Naaijen, and Jan Willem van Wingerden. A novel control architecture for floating offshore wind turbines. In *IFAC 22nd World Congress*, 2023.

[14] A. Hegazy, P. Naaijen, V. Leroy, F. Bonnefoy, M. R. Mojallizadeh, Y. Pérignon, and J.-W. van Wingerden. The potential of wave feedforward control for floating wind turbines: a wave tank experiment. *Wind Energy Science*, 9(8):1669–1688, 2024.

[15] Paul Fleming, Jan-Willem Wingerden, and Alan Wright. *Comparing State-Space Multivariable Controls to Multi-SISO Controls for Load Reduction of Drivetrain-Coupled Modes on Wind Turbines through Field-Testing*. 2012.

[16] Jason Jonkman. Definition of the floating system for phase iv of oc3. Technical report, National Renewable Energy Lab.(NREL), Golden, CO (United States), 2010.

[17] G.K.V. Ramachandran, A. Robertson, J.M. Jonkman, and M.D. Masciola. Investigation of response amplitude operators for floating offshore wind turbines. In *Proceedings of the 23rd International Offshore and Polar Engineering Conference*, pages ISOPE–I–13–106, June 2013.

[18] Boris Fischer. Reducing rotor speed variations of floating wind turbines by compensation of non-minimum phase zeros. 7(4):413–419, 2013.

Control design for floating wind turbines

Amr Hegazy[1], Peter Naaijen[2], and Jan-Willem van Wingerden[1]

[1]Delft Center for Systems and Control, TU Delft, Mekelweg 2, 2628 CD, Delft, The Netherlands
[2]Maritime and Transport Technology, TU Delft, Mekelweg 2, 2628 CD, Delft, The Netherlands

Correspondence: Amr Hegazy (a.r.hegazy@tudelft.nl)

Abstract. While the generator speed feedback control of onshore wind turbines, via the pitch controller to feather the blades, is well-established, ~~applying the same controllers to~~ employing the same controller gains with floating offshore wind turbines causes the turbines to become unstable. Such instability is attributed to the coupling between the nacelle fore-aft motion and the wind turbine controller, which makes the ~~floating~~ wind turbine negatively damped. The non-minimum phase zeros existing in the transfer function from the blade pitch to the generator speed impose a fundamental limitation on the closed-loop bandwidth, posing a challenge to the operation of the floating turbines. This paper gives an overview of the control strategies and their tuning techniques employed for floating wind turbines in the presence of the negative damping instability. It discusses the different available strategies. Moreover, we propose a new controller that can alleviate the adverse effects of the negative damping while preserving the standard proportional-integral control structure. Contrary to the multi-input-multi-output controllers that have been proposed, the proposed controller is more robust since it does not require additional signals of the floating platform, which makes controllers often sensitive to unmodelled dynamics. The controller is compared against the previously proposed controllers using the non-linear simulation tool, OpenFAST. The proposed controller excels in regulating generator speed, surpassing other controllers in performance. Additionally, it effectively mitigates the platform pitch in addition to the tower and blade loads. However, achieving a balance between power quality, actuator usage, and structural loading presents inherent trade-offs that need to be carefully addressed.

1 Introduction

Wind energy is essential to meeting the decarbonisation objectives of the European Union (EU) energy system, as it ensures delivering clean, affordable and secure electricity to various sectors, including households, industry and transport. Consequently, wind energy is expected to heavily contribute to the EU renewable energy targets~~. This is not surprising, especially when we know that in 2024, wind energy covered~~ , with wind energy already covering 19% of the EU's electricity demand ~~. No wonder the EU is regarded as a pioneer in wind energy. Accordingly, this~~ in 2024. This has seen the EU revising the renewable energy directive, which lays down a minimum ~~binding~~ target of 42.5% share of renewables by 2030 with an aspiration to reach 45%. This is 10.5% higher than the initial 32% target. Subsequently, the EU could fulfil its ambition of becoming climate-neutral by 2050 (European Commission, 2023).

As of 2025, Europe boasts a total installed wind capacity of approximately 285 gigawatts (GW), marking a significant expansion in the region's renewable energy infrastructure. Wind power accounts for almost 20% of Europe's electricity consumption

nowadays, and projections indicate that this figure could rise in the future. The EU aims to increase its wind capacity from 225 GW today to 350 GW by 2030, with a target of 425 GW to align with ambitious energy security goals (WindEurope, 2025). As for the other continents, similar trends are observed (GWEC, 2025).

Offshore wind offers significant advantages over onshore wind due to higher wind speeds and more consistent wind directions. Floating Offshore Wind Turbines (FOWTs) present unique opportunities as they can be deployed in deeper waters and farther from shore compared to bottom-fixed turbines. This expands the potential for offshore wind development in regions with deeper sea basins, such as the Mediterranean and the Atlantic. However, FOWTs face harsher environmental conditions than onshore turbines. Unlike onshore turbines, FOWTs are subjected to additional disturbances caused by waves, which contribute to increased structural loading on top of the loads induced by wind turbulence. As a result, FOWTs experience higher fatigue loads due to the added impact of waves (Saenz-Aguirre et al., 2022).

The cost of energy defines the potential of one type of energy source to be preferred over another, with the Levelised Cost Of Energy (LCOE) being the metric representing the average cost of generating electricity over the lifetime of a power-generating asset, expressed in monetary terms per unit of electricity. The main challenge facing the further deployment of FOWTs is their high LCOE. While modifications to their aerodynamic, hydrodynamic and structural design are applied to bring the LCOE down, the control system should not be overlooked~~as it can significantly~~ . Developing new control architectures can contribute to reducing the LCOE. Another approach is control co-design (Pao et al., 2024), which has proven to be highly effective.

From a control perspective, FOWTs present additional complexities compared to onshore turbines. The dynamics introduced by the floating platform make control more challenging. A notable concern is the negative damping effect (Nielsen et al., 2006), as applying a fixed-bottom controller to a floating wind turbine can significantly amplify the system's dynamic response, leading to large peak-to-peak oscillations. The simplest way to avoid closed-loop instability without modifying the conventional baseline controller structure is to detune the control gains such that the closed-loop response of the generator speed mode in isolation has a natural frequency below the platform pitch resonant frequency (Larsen and Hanson, 2007; Jonkman, 2008). However, this leads to a degradation in the reference tracking performance of the blade pitch controller as its ability to effectively respond to disturbances becomes restricted (Yu et al., 2018; Lemmer et al., 2020). Maintaining global detuning across all wind speeds sacrifices higher control bandwidths at higher wind speeds that do not suffer from this instability. Accordingly, it is reasonable to schedule the detuning at each wind speed separately (Yu et al., 2018, 2020; Lemmer et al., 2020; Stockhouse et al., 2024b).

Other methods explored in the literature involve incorporating extra feedback loops to counteract the instability arising from rotor-platform interactions. By utilising nacelle fore-aft velocity as feedback to adjust the existing baseline controller actuators, blade pitch (Jonkman, 2008; van der Veen et al., 2012; Fleming et al., 2014) and generator torque (Fischer, 2013; Fischer and Loepelmann, 2016) control inputs showed performance improvements could be achieved without the need for additional actuators. ~~A multi-loop feedback systemevaluation requires a Multi-Input, Multi-Output (MIMO) Transfer Function (TF) representation. Those multi-loop~~ Systems with more than one actuating control input and more than one sensor output may be considered as multivariable systems or Multi-Input-Multi-Output (MIMO) systems. The control objective for multivariable systems is to obtain a desirable behaviour of several output variables by simultaneously manipulating several

input channels. A FOWT is a MIMO system. To evaluate such a system, MIMO transfer function matrix is needed. In many FOWT control strategies~~in the literature often employ a compartmentalised feedback design, where individual control channels are separately tuned to achieve improved dynamic responses~~ , the feedback control loops are often designed separately in a decoupled format, with each control loop tuned to improve the response of a specific output~~. While this segmented tuning methodology remains widespread, inter-loop dynamic coupling inherent in MIMO architectures generates cross-channel interference phenomena, whereby localised parameter adjustment in a single control loop perturbs the closed-loop response characteristics of adjacent feedback channels.~~ (Fleming et al., 2012). This means that the multivariable controller design is reduced to a series of single-loop controllers. Although this approach is common, the loops in a MIMO system are dynamically coupled. As a result, changing the settings of one control loop can affect the behaviour of other loops, causing interaction between them. Subsequently, the interaction between the different control loops of a system should be dealt with simultaneously. It was demonstrated that improved performance could be achieved when optimally tuning all the control loops collectively, accounting for the interdependencies within the MIMO feedback structure rather than tuning each control loop independently (Stockhouse et al., 2024b). Modern multivariable control methodologies employing state-feedback architectures, including Linear Quadratic Regulator (LQR) (Namik et al., 2008) and $\mathcal{H}_\infty$ control (De Corcuera et al., 2012; Hegazy et al., 2023a) demonstrate systematic efficacy in achieving specified stability and performance envelopes for complex dynamical systems (Skogestad and Postlethwaite, 2005).

~~This paper provides a tutorial on~~

This paper addresses the design of closed-loop controllers for FOWTs~~, outlining various control strategies proposed in the literature. It also evaluates the performance of these strategies, particularly in addressing the negative damping instability. Additionally,~~ . We begin by outlining the fundamental principles of closed-loop control for FOWTs and describing how the negative damping problem arises. This instability has been widely recognised as a critical challenge, as it can compromise both performance and structural safety.

To provide context, we review existing control strategies proposed in the literature and assess their ability to mitigate the negative damping effect. Although these approaches have advanced the understanding of the problem, they often rely on additional sensors.

The main contribution of this paper is the introduction of a novel controller structure ~~is introduced, which~~ that eliminates the need for ~~additional sensors , along with a detailed tuning technique.~~ supplementary sensors while maintaining robust and reliable performance. A detailed tuning methodology is also presented to support practical deployment. Together, these contributions highlight a new pathway for addressing the negative damping problem in FOWTs and advancing the development of effective control solutions.

The remainder of this paper is structured as follows: In Section 2, the FOWT control problem is defined, and the control design model is introduced. In Section 3, conventional Single-Input, Single-Output (SISO) and MIMO control strategies are discussed. In Section 4, the controllers are evaluated by simulating the closed-loop system using the non-linear aero-servo-hydro-elastic tool OpenFAST (NREL, 2025a).

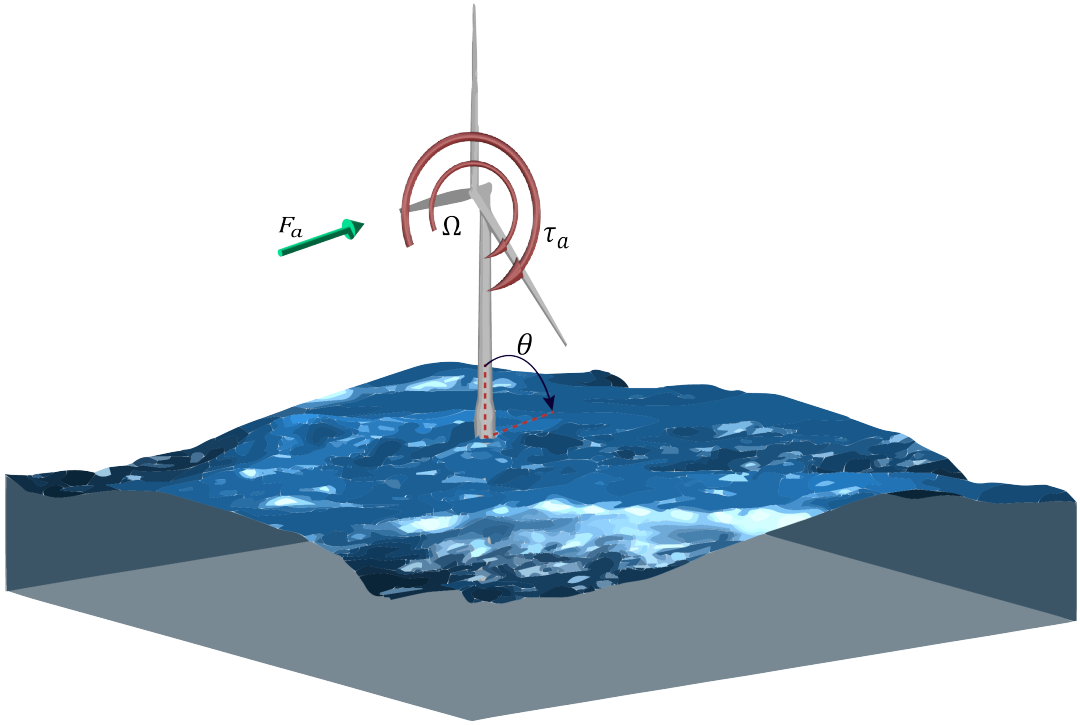

Figure 1. Schematic of the FOWT depicting the generator speed, Ω, and the platform pitch, θ, DoFs of the simple control model together with the external forces, namely, the aerodynamic thrust, F_a, and torque, τ_a, as expressed in Eq. (14).

2 Problem background

In this section, we start by introducing the dynamic model of a conventional fixed-bottom wind turbine. Afterwards, we go on to explain the process of closing the loop with the baseline controller and the tuning methodology of the controller gains. Once this is established, we move on to the FOWTs where we introduce the additional dynamics for the floating platform to form a representative dynamic model of a FOWT to conduct further analysis on the complexities that arise when controlling FOWTs.

Conventional wind turbine dynamics are excited by the imbalance between the aerodynamic torque and the generator torque, which drives the generator speed, and thus ~~,~~ a simplified wind turbine model is described as:

$$\frac{J_r}{N_{gb}}\dot{\Omega} = \tau_a(\Omega, \beta, v) - N_{gb}\tau_g, \tag{1}$$

where J_r (kg.m^2) is the rotor drivetrain inertia, Ω (rad.s^{-1}) is the generator speed with the dot notation indicating the time derivative, τ_a (N.m) is the aerodynamic torque, N_{gb} (-) is the gearbox ratio, and τ_g (N.m) is the generator torque. The aerody-

namic torque $\tau_a(\Omega, \beta, v)$ is modelled by a non-linear function:

$$\tau_a = \frac{1}{2}\rho\pi R^2 N_{gb} \frac{v^3}{\Omega} C_p(\lambda, \beta), \tag{2}$$

with ρ (kg.m^{-3}) as the air density, R (m) being the rotor radius, $C_p(\lambda, \beta)$ as the power coefficient, which depends on the blade pitch angle, β (rad), and the tip-speed ratio, $\lambda = \Omega R / v N_{gb}$, with v (m.s^{-1}) being the wind speed normal to the rotor plane. ~~Around an equilibrium point, $\bar{x}$, a perturbation state, δx, is defined as $\delta x = x - \bar{x}$, and a non-linear function $f(\bar{x}) = 0$. Therefore,~~ At steady-state, the non-linear wind turbine dynamics in Eq. (1) ~~, at steady-state,~~ can be linearised using first-order Taylor series expansion around an equilibrium point as:

$$\delta\dot{\Omega} = \frac{N_{gb}}{J_r}\left(\frac{\partial \tau_a}{\partial \Omega}\delta\Omega + \frac{\partial \tau_a}{\partial v}\delta v + \frac{\partial \tau_a}{\partial \beta}\delta\beta - N_{gb}\delta\tau_g\right), \tag{3}$$

where δ denotes state perturbation, and the partial derivatives of τ_a with respect to its independent variables are known as the aerodynamic sensitivities.

In practice, wind turbines are regulated with a generator speed controller, as at below-rated wind speeds, the controller is seeking to maximise the extracted power by keeping the collective blade pitch angle, β, constant while varying the generator torque, τ_g, as a function of the square of the generator speed, Ω, as follows (Bossanyi, 2000):

$$\tau_g = k_g \Omega^2, \tag{4}$$

with $k_g = 0.5\rho\pi R^2 (C_{p,max}/N_{gb}^3 \lambda_{opt}^3)$, being the generator-torque constant. The variable $C_{p,max}$ is the maximum power coefficient achieved at the optimal Tip-Speed Ratio (TSR), λ_{opt}, and at a specific constant blade pitch angle known as fine blade pitch angle. ~~Although simple,~~ It is fair to mention that the controller in Eq. (4) ~~operates under the assumption that~~ assumes a constant k_g ~~remains constant~~ throughout the wind turbine's lifetime. In reality, this is not the case, as it is influenced by modelling inaccuracies and assumption errors. To address this limitation, the TSR tracking controller has proven to be more effective and is widely adopted in the wind energy industry (Abbas et al., 2022; Brandetti et al., 2023).

At above-rated wind speeds (referred to as Region 3), a conventional wind turbine controller relies on the blade pitch to regulate the generator speed to its rated value, Ω_{rat}, while keeping the generator torque constant at its rated value (Bossanyi, 2000). As a result, generator power fluctuations are directly proportional to the oscillations occurring in the generator speed, $\delta\Omega = \Omega - \bar{\Omega}$. The collective blade pitch controller regulates the generator speed about its steady-state value, $\bar{\Omega} = \Omega_{rat}$, according to the following feedback control law (Jonkman et al., 2009; Abbas et al., 2022):

$$\delta\beta = k_p \delta\Omega + k_i \int \delta\Omega dt, \tag{5}$$

where k_p and k_i are the proportional and integral controller gains, respectively. To reach a description of the gains, the azimuth angle ψ is introduced as $\Omega = \dot{\psi}$ in Eq. (3) and Eq. (5). By combining both equations and focusing on the generator

speed terms, we derive a closed-loop system. When rewritten in the standard form of a second-order mass-spring-damper system, it becomes (Jonkman et al., 2009; Abbas et al., 2022):

$$\delta\ddot{\psi} + \underbrace{\frac{-N_{gb}}{J_r}\left(\frac{\partial \tau_a}{\partial \Omega} + \frac{\partial \tau_a}{\partial \beta}k_p\right)}_{2\zeta_c\omega_c}\delta\dot{\psi} + \underbrace{\frac{-N_{gb}}{J_r}\frac{\partial \tau_a}{\partial \beta}k_i}_{\omega_c^2}\delta\psi = 0. \tag{6}$$

~~Notice that the terms~~ Equation (3) represents the closed-loop system of the wind turbine in the above-rated region. Therefore, only the terms containing ψ and its derivatives are considered (Jonkman et al., 2009). The remaining terms are irrelevant to the control problem ~~in Eq. (3) were dropped and~~ and therefore do not appear in Eq. (6). Accordingly, we can parametrise the PI blade pitch controller gains (Abbas et al., 2022):

$$k_i = -\omega_c^2 \frac{J_r}{N_{gb}}\left(\frac{\partial \tau_a}{\partial \beta}\right)^{-1} \tag{7}$$

$$k_p = \left(-2\zeta_c\omega_c\frac{J_r}{N_{gb}} - \frac{\partial \tau_a}{\partial \Omega}\right)\left(\frac{\partial \tau_a}{\partial \beta}\right)^{-1} \tag{8}$$

Given a desired natural frequency, ω_c, and damping ratio, ζ_c, the PI controller gains can be computed ~~(Åström and Murray, 2021)~~ (Åström and Murray, 2021; Abbas et al., 2022). By defining the ω_c and ζ_c of the generator speed response, the dynamic response of the rotor to wind speed variations can be altered. The value of ω_c defines the bandwidth of the feedback controller. Typically, the controller bandwidth is chosen below the lowest structural natural frequency of the system to avoid interaction with lightly damped modes, leading to instability. The bandwidth should not include the Right Half Plane Zeros RHPZs existing in the wind turbine system as Leithead and Dominguez (2006) reported. As shown in Eq. (7) and Eq. (8), ~~the~~ their controller gains depend on the aerodynamic sensitivities, which significantly vary across operating points. As a result, the controller gains are scheduled at each operating point and modified during operation as the wind speed changes to maintain consistent closed-loop transient behaviour using a linear controller.

The main challenge associated with the control of FOWTs, within Region 3 concerns their fore-aft motion (Larsen and Hanson, 2007; Jonkman, 2008; van der Veen et al., 2012; Fischer, 2013). Therefore, it is critical to include floating platform dynamics in the control design model.

2.1 Floating wind turbine model

The main problem associated with the control of floating wind turbines concerns the ~~platform~~ pitch stability in ~~the above-rated wind speed regime~~ full load (van der Veen et al., 2012; Larsen and Hanson, 2007; Jonkman, 2008; Fischer, 2013). The effect of varying wind speed on the steady-state thrust, in the above-rated region, has to be considered in order to understand this problem. The above-rated ~~part~~ portion of the steady state thrust curve, shown in Figure 2, is defined as the thrust force

required at a given wind speed to produce rated power at rated generator speed (van der Veen et al., 2012). The steady-state blade pitch angle varies along the operating curve to ~~achieve constant generator torque~~ limit the aerodynamic torque and reduce the oscillation in the power production. The generator torque is kept constant instead of constant power ~~, since this~~ since this strategy limits the generator speed variations, hence, ~~reduced drive train~~ reduces drivetrain loads and pitch activity~~(Larsen and Hanson, 2007). The objective is to achieve a stable power production with less variations such that its total differential diminishes.~~ (Larsen and Hanson, 2007).

To form a FOWT mathematical model, the generic 1-DOF model of the wind turbine in Eq. (3) is combined with the floating platform dynamics. For the sake of explaining the negative damping problem analytically, only a 2-DOF FOWT model capturing the critical dynamics is used, where the platform pitch degree of freedom (DOF) is primarily considered to characterise platform dynamics, as the negative damping instability is most pronounced at the platform pitch eigenfrequency ~~(Jonkman, 2008)~~, where there is no damping from the mooring and vary little hydrodynamic damping leading to negative damping if the pitch control is fast (Larsen and Hanson, 2007; Jonkman, 2008). However, to preserve key dynamic couplings, the control model used for the control design must include additional modes that capture the most significant system dynamics, namely the platform's surge and heave, and the tower first fore-aft bending (Lemmer et al., 2020); otherwise, some interactions within the system may be overlooked (Yu et al., 2020). The non-relevant DOFs are neglected to avoid accounting for extra states, which would increase the complexity. For this analysis, the NREL 5-MW Reference Wind Turbine (RWT) (Jonkman et al., 2009) is mounted on top of the OC3 spar floater (Jonkman, 2010). Such analysis was performed in Stockhouse et al. (2024b); Stockhouse and Pao (2024); Stockhouse et al. (2024a) for different FOWT system.

The rigid floating platform pitch motion in still water, thus, affected by the aerodynamic thrust force only without any wave-induced forces, can be modelled as a second-order mass-spring-damper system:

$$I_p\ddot{\theta} + C\dot{\theta} + K\theta = l_h F_a(\Omega, v, \beta), \tag{9}$$

where θ is the platform pitch angle, $\dot{\theta}$ is the platform pitch rotational velocity, $\ddot{\theta}$ is the platform pitch rotational acceleration, I_p is the total mass moment of inertia about the platform pitch axis, comprising the structural inertia and the added mass associated with hydrodynamic radiation, C is the damping coefficient, K includes the hydrostatic and the mooring stiffnesses. Within the ~~simplified~~ analytical 2D model, the frequency-dependent radiation memory effects are disregarded by assuming a constant added mass and omitting radiation damping, as it is insignificant compared to viscous damping in FOWT platforms (Lemmer et al., 2016, 2020), while for the control model used for controller synthesis, a parametric radiation model is used (Perez and Fossen, 2009; Fontanella et al., 2020). However, for the time-domain simulations, the convolution integral (Cummins, 1961) is incorporated to account for the frequency-dependent coefficients. The variable F_a is the aerodynamic rotor thrust force, which causes a pitching moment on the platform through the hub height, l_h, as a lever arm. The aerodynamic thrust force $F_a(\Omega, \beta, v)$ is a non-linear function is expressed by:

$$F_a = \frac{1}{2}\rho\pi R^2 v^2 C_t(\lambda, \beta), \tag{10}$$

where v is the rotor effective wind speed, C_t is the thrust coefficient function in λ and β. The platform pitch motion influences the dynamics as it induces a relative wind speed at the rotor apart from the inflow wind speed, v_∞. Thus, the rotor effective wind speed, v, is:

$$v = v_\infty - l_h\dot{\theta}. \tag{11}$$

Similar to Eq. (3) while considering Eq. (11), the non-linear platform dynamics can be linearised around an equilibrium point as:

$$I_p\delta\ddot{\theta} + C\delta\dot{\theta} + K\delta\theta = l_h\left(\frac{\partial F_a}{\partial\Omega}\delta\Omega - l_h\frac{\partial F_a}{\partial v}\delta\dot{\theta} + \frac{\partial F_a}{\partial\beta}\delta\beta\right) \tag{12}$$

In a standard second-order form, by considering only the coefficients corresponding to the platform pitch motion, Eq. (12) can be rewritten as:

$$\delta\ddot{\theta} + \underbrace{\frac{1}{I_p}\left(C + l_h^2\frac{\partial F_a}{\partial v}\right)}_{2\zeta_p\omega_p}\delta\dot{\theta} + \underbrace{\frac{K}{I_p}}_{\omega_p^2}\delta\theta = 0, \tag{13}$$

with ω_p and ζ_p being the natural frequency and the damping ratio of the floating platform in the pitch DoF, respectively.

The coupled dynamics of the wind turbine in Eq. (3) and the floating platform in Eq. (12) form a third-order system, which is represented in state space form of $\dot{\boldsymbol{x}} = \boldsymbol{A}\boldsymbol{x} + \boldsymbol{B}\boldsymbol{u}$, with a state vector $\boldsymbol{x} = [\theta\ \dot{\theta}\ \Omega]^\top$, and control input vector $\boldsymbol{u} = [\tau_g\ \beta]^\top$, as:

$$\dot{\boldsymbol{x}} = \begin{bmatrix} 0 & 1 & 0 \\ -\frac{K}{I_p} & -\frac{1}{I_p}\left(C + l_h^2\frac{\partial F_a}{\partial v}\right) & \frac{l_h}{I_p}\frac{\partial F_a}{\partial\Omega} \\ 0 & -l_h\frac{N_{gb}}{J_r}\frac{\partial\tau_a}{\partial v} & \frac{N_{gb}}{J_r}\frac{\partial\tau_a}{\partial\Omega} \end{bmatrix}\boldsymbol{x} + \begin{bmatrix} 0 & 0 \\ 0 & \frac{l_h}{I_p}\frac{\partial F_a}{\partial\beta} \\ -\frac{N_{gb}^2}{J_r} & \frac{N_{gb}}{J_r}\frac{\partial\tau_a}{\partial\beta} \end{bmatrix}\boldsymbol{u}, \tag{14}$$

~~where the individual elements of the system matrix, $\boldsymbol{A}$, and the input matrix, $\boldsymbol{B}$, are defined in Table ??.~~ The output vector $\boldsymbol{y} = \boldsymbol{C}\boldsymbol{x} + \boldsymbol{D}\boldsymbol{u}$, with the output matrix $\boldsymbol{C}$ and the feed-through matrix $\boldsymbol{D}$, is defined according to the available system measurements, which is typically a subset of the states in the state vector $\boldsymbol{x}$. In this paper, the output vector is chosen as $\boldsymbol{y} = [\dot{\theta}\ \Omega]^\top$, and thus obtained for the state-space model in Eq. (14) as:

$$\boldsymbol{y} = \begin{bmatrix} 0 & 1 & 0 \\ 0 & 0 & 1 \end{bmatrix}\boldsymbol{x}, \tag{15}$$

~~The element A_{θ}^{Ω} in the system matrix, $\boldsymbol{A}$, in Eq. (14) is the state transition term from the platform pitch velocity, $\delta\dot{\theta}$, to the generator acceleration, $\delta\dot{\omega}_g$, which clearly shows the direct effect of the platform pitch motion on the generator acceleration via the term $\frac{-1}{J_r}\frac{\partial \tau_a}{\partial v}$.~~

~~The elements of the system matrices $\boldsymbol{A}$ and $\boldsymbol{B}$. **Element** **Definition** A_K^{θ} $\frac{K}{I_p}$ A_C^{θ} $\frac{1}{I_p}\left(C + l_h^2\frac{\partial F_a}{\partial v}\right)$ A_{Ω}^{θ} $\frac{l_h}{I_p}\frac{\partial F_a}{\partial \Omega}$ A_{θ}^{Ω} $-l_h\frac{N_{gb}}{J_r}\frac{\partial \tau_a}{\partial v}$ A^{Ω} $\frac{N_{gb}}{J_r}\frac{\partial \tau_a}{\partial \Omega}$ B_{β}^{θ} $\frac{l_h}{I_p}\frac{\partial F_a}{\partial \beta}$ $B_{\tau_g}^{\Omega}$ $\frac{N_{gb}^2}{J_r}$ B_{β}^{Ω} $\frac{N_{gb}}{J_r}\frac{\partial \tau_a}{\partial \beta}$~~

Now with such linear state space model, we can view the problem analytically with a pole-zero plot, shown in Fig. 3, of the TF, $G_{\Omega,\beta}$, mapping the collective pitch pitch, β, to generator speed, Ω, describing how generator speed (controlled variable) responds to a variation in blade collective pitch angle (control input). First, let us look at the analytical description of $G_{\Omega,\beta}$. This requires transferring to the frequency domain, which can be attained by applying $\boldsymbol{G}(s) = \boldsymbol{C}(s\boldsymbol{I} - \boldsymbol{A})^{-1}\boldsymbol{B} + \boldsymbol{D}$, with s being the Laplace variable, and $\boldsymbol{I}$ being the identity matrix. As a result, we get a MIMO transfer function matrix, $\boldsymbol{G}(s) = \boldsymbol{G_{uy}}(s)$, mapping the input vector $\boldsymbol{u}$ to the output vector $\boldsymbol{y}$. The transfer function matrix $\boldsymbol{G}(s)$ is composed of SISO TF $G_{u_i y_i}(s) = y_i(s)/u_i(s)$ mapping each input $u_i(s)$ to each output $y_i(s)$:

$$\boldsymbol{G}(s) = \begin{bmatrix} G_{\dot{\theta},\tau_g} & G_{\dot{\theta},\beta} \\ G_{\Omega,\tau_g} & G_{\Omega,\beta} \end{bmatrix} \tag{16}$$

For the feedback control of FOWTs ~~, the~~ in Region 3, the control objective is to reduce the generator speed oscillations using the blade pitch action. Consequently, the TF, $G_{\Omega,\beta}$, mapping the blade pitch angle to the generator speed, in Eq. (16) is of the main interest:

$$G_{\Omega,\beta} = \frac{\frac{\partial \tau_a}{\partial \beta}\left(I_p s^2 + \left[C + l_h^2\frac{\partial F_a}{\partial v}\right]s + K\right) - l_h^2\frac{\partial \tau_a}{\partial v}\frac{\partial F_a}{\partial \beta}s}{\left(\frac{J_r}{N_g b}s - \frac{\partial \tau_a}{\partial \Omega}\right)\left(I_p s^2 + \left[C + l_h^2\frac{\partial F_a}{\partial v}\right]s + C\right) + l_h^2\frac{\partial \tau_a}{\partial v}\frac{\partial F_a}{\partial \Omega}s}, \tag{17}$$

where all the gradients vary with the operating point. To determine the zeros of $G_{\Omega,\beta}$, its numerator polynomial is set to zero, and the resulting equation is solved for s using the quadratic formula. Upon algebraic manipulation, it becomes evident that RHPZs, indicating non-minimum phase behaviour, emerge under the following condition (Fischer, 2013):

$$C < -l_h^2\underbrace{\left[\frac{\partial F_a}{\partial v} - \frac{\partial \tau_a}{\partial v}\frac{\partial F_a}{\partial \beta}\left(\frac{\partial \tau_a}{\partial \beta}\right)^{-1}\right]}_{\mu_{aero}} \tag{18}$$

Equation (18) highlights that the emergence of non-minimum phase behaviour, driven by the presence of RHPZs, is closely tied to the aerodynamic damping coefficient (μ_{aero}), which is influenced by aerodynamic gradients. This coefficient varies with the operating conditions and tends to be particularly low near the rated wind speed, as will be demonstrated in the following analysis.

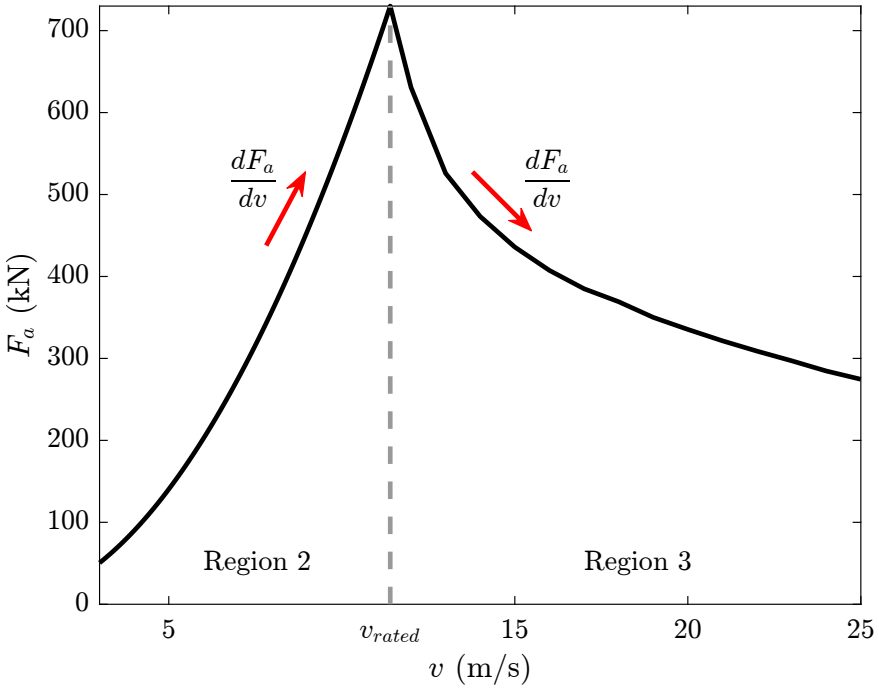

Figure 2. Steady-state values of rotor thrust force, F_a, as a function of the effective rotor wind speed, v, for the NREL 5-MW baseline wind turbine on OC3 spar floating platform.

Figure 2 illustrates the relationship between the steady-state aerodynamic thrust force (F_a) and the rotor-effective wind speed (v) for the above-rated operation of the NREL 5-MW reference wind turbine (Jonkman et al., 2009) installed on the OC3 spar floating platform (Jonkman, 2010). ~~Under the assumption of quasi-static equilibrium, where system variables are balanced for each wind speed~~In a closed-loop FOWT system at steady state, the gradient dF_a/dv is positive below-rated wind speed, meaning the thrust force increases as wind speed rises. However, beyond the rated wind speed, this gradient becomes negative, as shown in Fig. 2. This behaviour results from the pitch-to-feather control strategy, which reduces aerodynamic loads ~~and modifies the force direction~~ in the above-rated region. As a consequence, the aerodynamic damping is positive at below-rated wind speeds but turns negative at above-rated wind speeds. As F_a begins with a positive slope ($\mu_{aero} > 0$) in Region 2, where F_a keeps increasing till reaching its maximum at the rated wind speed where $\mu_{aero} = 0$. Once Region 3 is reached, F_a starts decreasing with a significantly steep negative slope ($\mu_{aero} < 0$). The steeper this decline, the lower the aerodynamic damping, with its minimum occurring just beyond the rated wind speed. As wind speed continues to increase, the slope gradually becomes less steep, indicating a partial recovery of aerodynamic damping.

The root cause of this behaviour is the negative total derivative of thrust force with respect to above-rated wind speeds (Fischer, 2013) as in Region 3, the rotor speed (Ω_r) is at its constant rated value, while the aerodynamic torque (τ_a) varies. The objective is to achieve stable power production (P) with fewer variations such that its total differential diminishes (van der Veen et al., 2012):

$$dP = \Omega_r d\tau_a = \Omega_r \left(\frac{\partial \tau_a}{\partial v} dv + \frac{\partial \tau_a}{\partial \beta} d\beta \right) = 0, \tag{19}$$

and from Eq. (19), the total differential of the blade-pitch angle is:

$$d\beta = -\frac{\partial \tau_a}{\partial v} \left(\frac{\partial \tau_a}{\partial \beta} \right)^{-1} dv \tag{20}$$

Similar to $d\tau_a$ in Eq.(19), the total differential of F_a is:

$$dF_a = \frac{\partial F_a}{\partial v} dv + \frac{\partial F_a}{\partial \beta} d\beta \tag{21}$$

Combining Eq. (20) and Eq. (21), the total derivative of the aerodynamic thrust with respect to the wind speed, yielded from the variation of blade pitch to maintain rated power, is:

$$\frac{dF_a}{dv} = \frac{\partial F_a}{\partial v} - \frac{\partial F_a}{\partial \beta} \frac{\partial \tau_a}{\partial v} \left(\frac{\partial \tau_a}{\partial \beta} \right)^{-1} = \mu_{aero} \tag{22}$$

Equation (22) demonstrates why F_a has a negative gradient, $dF_a/dv < 0$, as wind speed increases, a condition that is necessarily true for all conventional pitch-to-feather wind turbines (van der Veen et al., 2012). Burton et al. (2021) explains that as the wind increases above-rated, the pitch angle increases to maintain constant generator torque, but the aerodynamic thrust and torque decrease, indicating that the gradients $\partial F_a/\partial \beta$ and $\partial \tau_a/\partial \beta$ are negative. This allows the downwind fore-aft motion to decrease, which leads to an upwind fore-aft motion, causing the relative wind speed seen by the rotor to increase. Consequently, the aerodynamic torque increases further, causing more pitch action (Jonkman, 2008; van der Veen et al., 2012). So, the gradient $\partial \tau_a/\partial v$ is positive. Therefore, after considering the signs of all the gradients in Eq. (22), it becomes clear why $dF_a/dv < 0$ in the above-rated operation.

After obtaining $G_{\Omega,\beta}$ from $G(s)$ in Eq. (16), the pole-zero map of $G_{\Omega,\beta}$, that maps the blade collective pitch, β, to the generator speed, Ω, describing how the generator speed responds to a variation in blade pitch angle, is shown in Fig. 3.

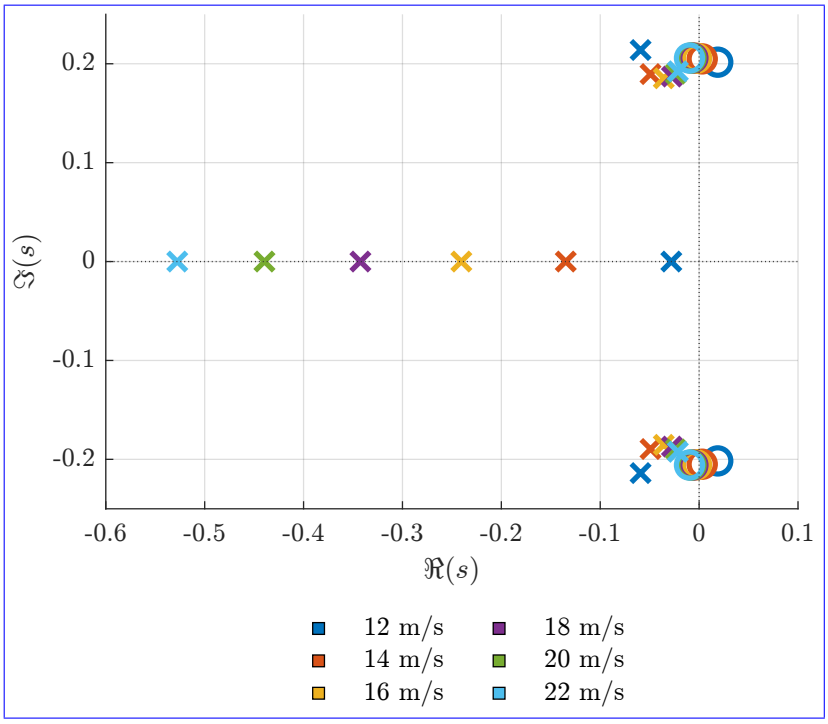

Figure 3. Pole-Zero map of the TF from blade collective pitch to rotor speed, $G_{\Omega,\beta}$, at different operating points. Poles and zeros are denoted by $\times$ and $\circ$, respectively.

Figure 3 shows that the TF, $G_{\Omega,\beta}$, consists of a complex pole pair, corresponding to the platform rigid-body pitch mode, and a real pole, associated with the drivetrain mode. Additionally, a complex pair of RHPZ appears at a frequency close to that of the platform pitch mode, indicating that the RHPZs condition in Eq. (18) is satisfied. The poles in the platform pitch mode of the open-loop transfer function, $G_{\Omega,\beta}$, correspond to the pitch-free decay damping ratio, ζ_p, and natural frequency (eigen-frequency), ω_p. It can be seen in Fig. 3 that the open-loop system is originally stable because of the sufficient hydrodynamic damping (Yu et al., 2018) since all the poles are in the left-half-plane (LHP).

However, the closed-loop poles of a system would migrate from the open-loop poles location towards the open-loop zeros as the feedback gain increases (van der Veen et al., 2012). Hence, according to Fig. 3, the platform pitch mode becomes less damped, whilst the generator speed tracking improves. In the case where the zeros are in the right half plane, which for the model visualized in Fig. 3 is true only for the platform pitch zeros, the frequencies provide bandwidth limits on $G_{\Omega,\beta}$ loop.

2.2 Effect of RHP zeros

The roots of the numerator of a transfer function are called zeros (denoted by ◯ in Fig. 3). A zero represents a critical frequency, referred to as the frequency of the zero, where the input signal is entirely blocked and has no effect on the system's output. In particular, RHPZs exhibit an "inverse-response behaviour," meaning the system output initially moves in the opposite direction

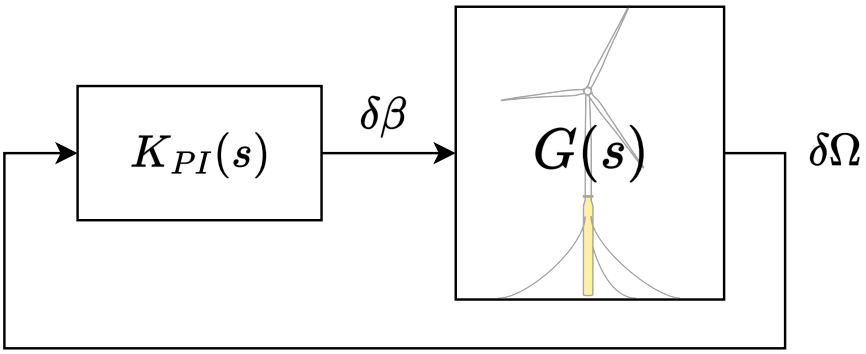

Figure 4. Block diagram of the FOWT closed loop system, where $G(s)$ represents the plant model, and $K_{PI}(s)$ represents the collective blade pitch controller.

of the expected response (Skogestad and Postlethwaite, 2005). This unique characteristic imposes strict constraints on control system design, especially in single-input single-output (SISO) configurations (Lemmer et al., 2016). Additionally, when the system is excited at or near the frequency of the zero, the risk of instability increases significantly. To mitigate this, limiting the controller bandwidth below the smallest RHPZ frequency is a must (Skogestad and Postlethwaite, 2005).

The effects of RHPZs extend beyond simple instability risks. As detailed in (Doyle et al., 2013), RHPZs introduce phase loss, which diminishes the performance of closed-loop systems as the zero frequency approaches the loop's cross-over frequency. This degradation becomes more critical in systems with weakly damped zeros (characterised by low damping ratios, ζ), where abrupt phase shifts occur near the zero frequency, ω_z. Such phase shifts are particularly problematic when the RHPZ frequencies fall below the controller bandwidth or the loop transfer function's cross-over frequency, exacerbating instability risks and limiting achievable performance. From a control design standpoint, RHPZs are universally undesirable due to their adverse impact on system stability and the fundamental limitations they impose on the achievable closed-loop bandwidth. Therefore, a careful balance between system performance and the trade-offs introduced by RHPZs should be considered, ensuring that controller bandwidth is appropriately tuned to account for these limitations.

3 Control of floating wind turbines

This section reviews various control strategies proposed for mitigating the negative damping instability in FOWTs, beginning with the most straightforward approaches and progressing toward more complex solutions involving additional sensors and actuators. Each method is evaluated in terms of its ability to address the negative damping effect and its effectiveness in overcoming the bandwidth limitation imposed by the RHPZs. Ultimately, the analysis concludes that only the incorporation of an additional actuator can effectively alleviate the constraint on closed-loop bandwidth.

Figure 4 shows the block diagram of the closed-loop FOWT system with the simple feedback PI controller. Each block represents a linear TF, with $G(s)$ mapping β, the collective blade pitch angle, to Ω, the generator speed, while $K_{PI}(s)$ is the collective blade pitch controller.

Neglecting the floating platform dynamics during the FOWT control design often yields instability in the operating points containing RHPZs. ~~This is because~~ As the high control bandwidth, associated with the high feedback control gains, causes platform pitch excitation (Jonkman, 2008). At first, one might expect exponential growth in the response due to negative damping, but this is not the case because of the non-linear dynamic coupling between the different FOWT modes. Yet the FOWT keeps oscillating back and forth without reaching a steady state, which is still undesirable. There are several ways to mitigate this challenging problem. Thus, in the remainder of this section, the conventional solutions are presented, followed by our proposed solution in the next section.

3.1 Detuning

A common approach to mitigating negative damping instability is to reduce the bandwidth of the blade pitch controller below the platform's natural frequency (Larsen and Hanson, 2007; Jonkman, 2008; van der Veen et al., 2012). While this stabilises the system, it compromises generator speed tracking performance at operating points where detuning is implemented.

Detuning introduces a control performance trade-off in the vicinity of rated wind speeds. Lowering the closed-loop bandwidth to maintain stability compromises the system's disturbance rejection capability and degrades power tracking performance.

3.2 Robust scheduled tuning

As previously mentioned, stability can be maintained in the presence of RHPZs by detuning, such that the natural frequency of the closed-loop is below the frequency of the RHPZs, which is approximately equal to the resonant frequency of the platform pitch (Lemmer et al., 2020). Applying ~~this~~ the global detuning approach means that the bandwidth and the damping ratio are constant across all the operating points, which is inefficient since it sacrifices better tracking performance. According to Fig. 2 and Fig. 3, the limitation set by the RHPZs varies according to the operating point.

~~Instead of the global detuning explained~~ Rather than applying a global detuning strategy at all the operating points as described in the previous section, a more ~~efficient approach is to detune~~ effective method involves individually tuning the PI controller ~~to the fastest possible~~ for the fastest achievable response at each operating point~~separately while maintaining~~ , while still ensuring the stability of the linear system ~~(Lemmer et al., 2020; Yu et al., 2020; Stockhouse et al., 2024b). In practice, it is not enough that a system is stable. There must also be some margins of stability that describe how far from instability the linear system is and its robustness to perturbations~~(Lemmer et al., 2020; Yu et al., 2020; Stockhouse et al., 2024b; Stockhouse and Pao, 2024) . However, achieving a stable system is not sufficient in control design; the system must also exhibit adequate stability margins, which indicate how close it is to instability and how robust it is to disturbances. The gain and phase margins are classical robustness measures that have been used for a long time in control system design, but they are not always good robustness indicators when it comes to the Nyquist stability criterion. However, the stability margin s_m can be used instead to give a more

general robustness measure. On one hand, it unites both the gain and phase margins under a single parameter, while on the other hand, it ensures that the Nyquist stability criterion is met. The stability margin s_m is also a good robustness measure of nominally stable systems against model uncertainties. The stability margin of a closed-loop system is defined as the shortest distance between the Nyquist curve of the system's loop transfer function, $L(s) = G(s)K(s)$, and the critical point at $s = -1$ in the s-plane, and it expresses how well the Nyquist curve of the loop transfer avoids the critical point. While there is no representation of s_m in the Bode plot of the loop transfer function, s_m is related to the the peak magnitude, M_s, of the sensitivity closed-loop transfer function, $S(s) = (1 + L(s))^{-1}$, through $s_m = 1/M_s$, and M_s being the $\mathcal{H}_\infty$ norm of $S(s)$ as (Åström and Murray, 2021):

$$s_m = \frac{1}{M_s} = \frac{1}{\|S(s)\|_\infty} \tag{23}$$

System stability robustness is a critical design priority for FOWTs, often leveraged in prior studies to calibrate both SISO (Lemmer et al., 2020) and MIMO control architectures ~~(Stockhouse et al., 2024b)~~(Stockhouse et al., 2024b; Stockhouse and Pao, 2024) . The contour plots in Fig. 5 and Fig. 6 depict the stability margin and the closed-loop bandwidth evaluated over a range of the Proportional-Integral (PI) control parameters, namely, the natural frequency (ω_c ~~and~~) and the damping ratio (ζ_c), showcasing the stable design space of the controller parameters, with the white-coloured region determining the unstable region. The stable region becomes larger as wind speed increases and the effect of the RHPZs fades according to Fig. 3, which allows for more freedom to increase the controller gains and thus increase the closed-loop bandwidth without destabilising the system. It is important to mention that a stable design space means that the combination of the control parameters means a stable closed-loop system (i.e. not having right-half plane poles). Although the stable design space is extended at higher wind speeds, some combinations of the controller parameters would significantly increase the controller aggressiveness, leading to instability in the non-linear simulations.

Increasing the closed-loop bandwidth reduces the stability margin, pushing the system closer to instability, as shown in Fig. 5 and Fig. 6. Consequently, achieving robust tuning of the PI controller requires a trade-off between stability robustness and closed-loop bandwidth, as these are competing objectives. ~~An~~ Inspired by the work done in Lemmer et al. (2020); Stockhouse et al. (2024b) , an optimisation-based tuning integrating the two key system properties: the stability margin and the closed-loop system bandwidth while considering the actuator limits, is thus employed. The PI controller is parametrised by ~~ω_p~~ ω_c and ζ_c collected in the vector $\mathbf{x} \in \mathbb{R}^2$. A scalar objective function $J(\mathbf{x}) : \mathbb{R}^2 \to \mathbb{R}$ is then constructed with the following requirements~~,~~: (i) maximise robust stability margin, (ii) maximise closed-loop bandwidth, and (iii) maintain acceptable actuator activity. When formulating $J(\mathbf{x})$, an important aspect is considering the actuator activity to avoid saturation. The control sensitivity function, $K(s)S(s)$, is a good indicator of the actuator activity. Inspired by s_m, the control effort margin s_c is introduced here as a measure of actuation robustness. A low s_c indicates high sensitivity to disturbances, risking actuator saturation. Analogous to s_m, we propose the variable s_c that is related to the peak magnitude of the control sensitivity function M_c through $s_c = 1/M_c$, where M_c is defined as $M_c = \|K(s)S(s)\|_\infty$. The objective function is then formulated as:

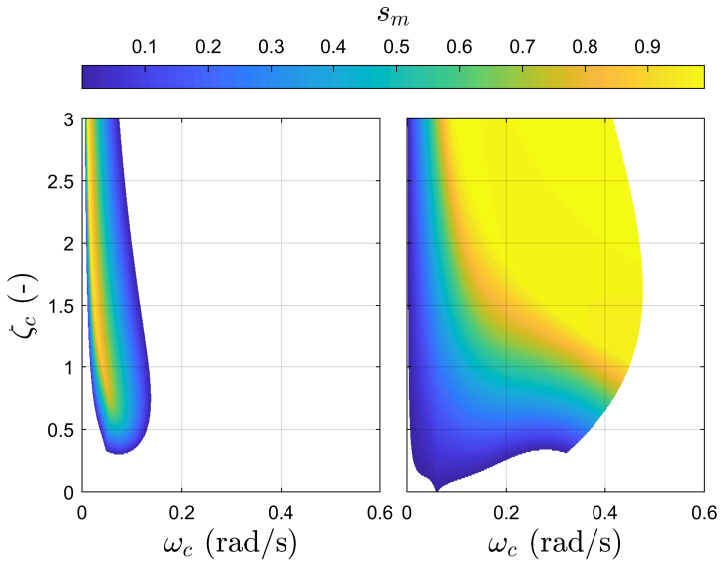

Figure 5. Stability margin contours across the natural frequency ω_c and damping ratio ζ_c of the PI controller, shown at two different operating points; near-rated ($\bar{v}$ = 13 m/s) and near cut-out ($\bar{v}$ = 24 m/s) wind speeds. The white region indicates a destabilising combination of ω_c and ζ_c.

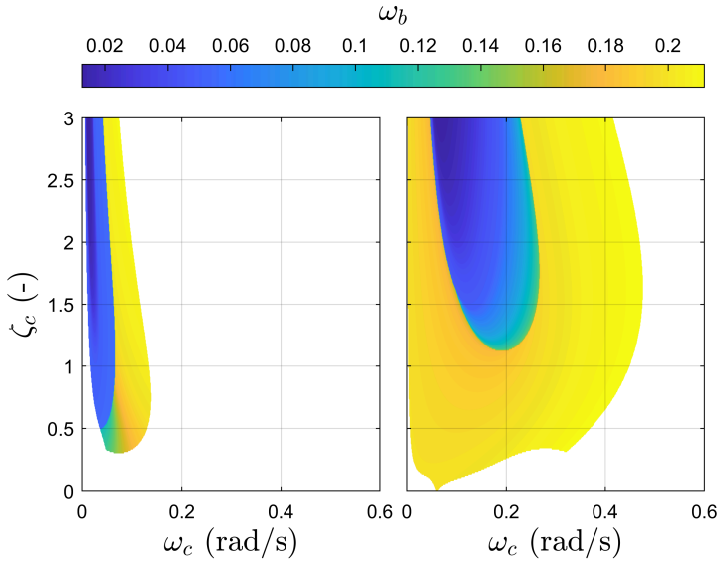

Figure 6. Closed-loop bandwidth contours across the natural frequency ω_c and damping ratio ζ_c of the PI controller, shown at two different operating points; near-rated ($\bar{v}$ = 13 m/s) and near cut-out ($\bar{v}$ = 24 m/s) wind speeds. The white region indicates a destabilising combination of ω_c and ζ_c.

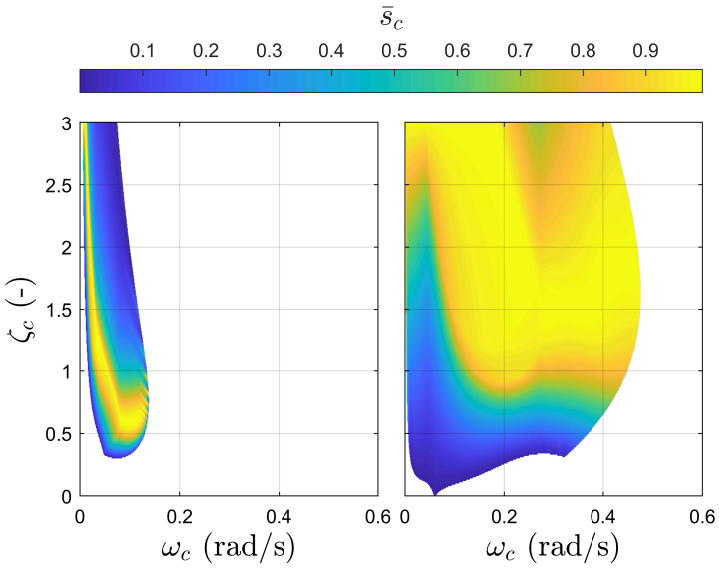

Figure 7. Control effort margin contours across the natural frequency ω_c and damping ratio ζ_c of the PI controller, shown at two different operating points; near-rated ($\bar{v}$ = 13 m/s) and near cut-out ($\bar{v}$ = 24 m/s) wind speeds. The white region indicates a destabilising combination of ω_c and ζ_c.

$$J(\mathbf{x}) = \mathrm{w}_{\mathrm{s_m}} s_m(\mathbf{x})^{-1} - \mathrm{w}_{bw}\omega_b(\mathbf{x}) + \mathrm{w}_{s_c} s_c(\mathbf{x})^{-1}, \tag{24}$$

where w_{s_m}, w_{bw}, and w_{s_c} are weights adjusting the importance of the stability margin, the bandwidth, and the control effort margin, respectively. Regularisation terms may be added to the objective function to fulfil control objectives such as minimising the generator speed and power oscillations, as well as reducing the loads (lem), and limiting the control gains (Stockhouse and Pao, 2024). Despite acknowledging that regularisation terms may be added to limit the gains, Stockhouse and Pao (2024) do not explicitly integrate actuator limits within their objective function formulation. Neglecting the actuator limits in the objective function would result in controller saturation. Conversely, Eq. (24) explicitly incorporates this constraint, ensuring the controller remains within operational limits. The objective function in Eq.(24) is then implemented in the optimisation problem in the form:

$$\mathbf{x} = \underset{\mathbf{x}}{\operatorname{argmin}}\, J(\mathbf{x}) \tag{25}$$

In this framework, the optimisation variables (denoted as $\mathbf{x}$) are the tuning parameters influencing three critical system properties: the stability margin, the closed-loop bandwidth, and the control effort margin. A systematic tuning method, leveraging the simplified dynamic system, enables rapid recalibration of control settings and assessment of steady-state behaviour. The

core objective is to maximise the closed-loop bandwidth while minimising the inverse of the stability margin. Focusing on the inverse of the stability margin ensures the closed-loop stability of the system, while parameters that cause instability are dropped out. After formulating and weighting the objective function, a locally optimal solution is derived using a gradient-based optimisation solver.

Based on Eq. (24) and according to Fig.5 and Fig. 6, we have two competing objectives, as an increase in the closed-loop bandwidth leads to a reduction in the closed-loop stability margin. Therefore, tuning the PI controller gains to achieve both objectives is not trivial, especially since finding a globally optimal solution is not guaranteed with gradient-based optimisation. Accordingly, a multi-objective optimisation problem is formulated over a set of continuous input variables $\mathcal{X} \subset \mathbb{R}^d$ called the d-dimensional design space (Lukovic et al., 2020). The optimisation goal is to maximise both the stability margin and the closed-loop bandwidth ~~. The optimisation goal is to minimise~~ through minimising the vector of the objectives defined as $f(x) = [f_1(x), \cdots, f_n(x)]$ with $n \geq 2, x \in \mathcal{X}$ being the vector of input variables and $f(\mathcal{X}) \subset \mathbb{R}^n$ the m-dimensional image representing the performance space.

The conflicting nature of the objectives does not always allow for the finding of a single optimal solution to the maximisation problem but a set of optimal solutions as shown in Fig. 8, referred to as the Pareto set $\mathcal{P}_s \subseteq \mathcal{X}$ in the design space and the Pareto front $\mathcal{P}_f = f(\mathcal{P}_s) \subset \mathbb{R}^n$ in the performance space (Lukovic et al., 2020).

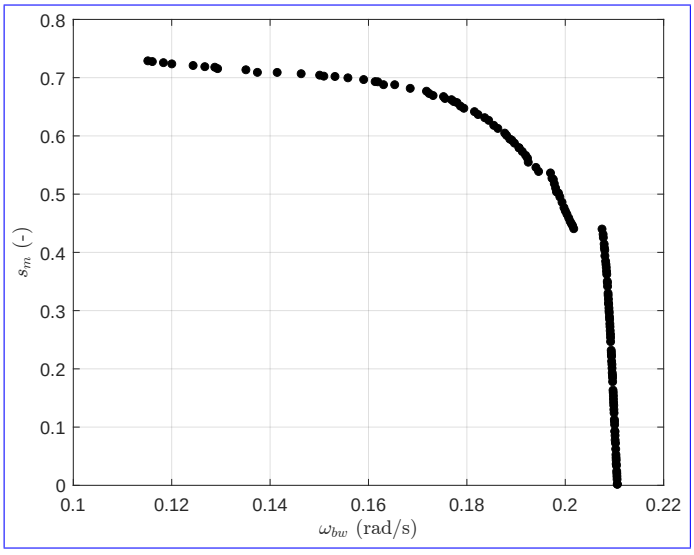

Figure 8. The Pareto front resulting from the multi-objective optimisation. Each data point indicates an optimal combination of the PI controller parameters ω_c and ζ_c.

The Pareto front in Fig. 8 clearly illustrates the trade-off between closed-loop stability and bandwidth. Beyond a certain threshold, further increasing the bandwidth significantly compromises system stability. The knee point on the Pareto front represents an optimal balance between these competing objectives, making it a ~~favorable~~ favourable region for selection. However, caution is needed when considering solutions in the upper-right region of the Pareto front. While they offer higher

Table 1. Robustly-scheduled control gains of the PI controller for the NREL 5 MW RWT.

v (m/s)	12	14	16	18	20	22	24
k_p (s)	0.0043	0.0037	0.0035	0.0036	0.0029	0.003	0.0048
k_i (-)	1.15E-04	9.97E-05	1.18E-04	1.31E-04	2.46E-04	2.89E-04	2.48E-04

bandwidth, they also lead to excessive pitch activity, rendering them impractical due to actuator constraints. The control gains used in this work are tabulated in Table 1.

3.3 Multi-loop control

A standard method to address negative damping instability involves implementing a secondary feedback loop that incorporates the platform pitch velocity signal. This technique can utilise blade pitch~~actuation~~ (van der Veen et al., 2012) or generator torque actuation (Fischer, 2013), representing a shift toward MIMO control strategies. The approach seeks to reduce the coupling between competing aerodynamic forces—rotor torque and thrust—while maintaining generator speed regulation via blade pitch adjustments. In this work, the platform pitch rate is employed as the fore-aft velocity signal for the secondary feedback loop. The study evaluates both blade pitch damping and generator torque for parallel compensation, finding that combining the two actuators balances their advantages and limitations.

In Eq. (14) of the state-space model, the matrix element ~~A^{Ω}_{θ}~~ $A(3,2)$ represents the dynamic coupling between platform pitch velocity, $\dot{\theta}$, and rotor acceleration, $\dot{\Omega}$. Nullifying this term diminishes the influence of platform pitching on rotor speed tracking. This tuning strategy does not directly suppress platform motion but counteracts its destabilizing effect on speed regulation, thereby enhancing closed-loop stability.

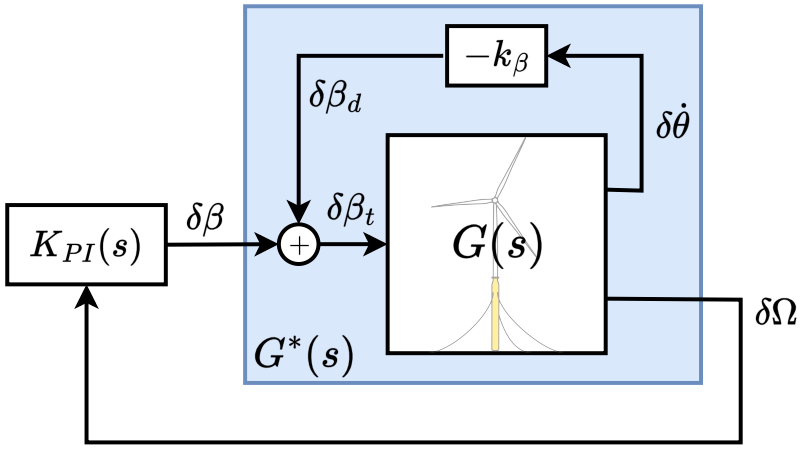

Figure 9. Block diagram of the ~~blade pitch damping (~~MISO controller ~~)~~with the additional blade pitch loop.

3.3.1 ~~Blade~~ Additional blade pitch ~~damping~~loop: MISO control structure

Compensation using blade pitch feedback, as shown in Fig. 9, is achieved by adding an extra term to the element ~~A^{Ω}_{θ}~~ $A(3,2)$, corresponding to the closure of the inner loop, where the static gain, k_β, is scheduled to be consistent with the PI controller gains for each operating point. The blade pitch damping approach uses proportional feedback of the platform pitch velocity (Jonkman, 2008; van der Veen et al., 2012):

$$\delta\beta_d = -k_\beta \dot{\theta} \tag{26}$$

Therefore, the overall blade pitch signal becomes:

$$\delta\beta_t = \delta\beta + \delta\beta_d \tag{27}$$

Closing the inner feedback blade pitch loop by substituting $\delta\beta$ from Eq. (27) in Eq. (3) and Eq. (12), the system matrix of the inner loop, $\boldsymbol{A^*}$, becomes:

$$\boldsymbol{A^*} = \begin{bmatrix} 0 & 1 & 0 \\ -\dfrac{K}{I_p} & -\dfrac{1}{I_p}\left(C + l_h^2\dfrac{\partial F_a}{\partial v} + l_h k_\beta \dfrac{\partial F_a}{\partial \beta}\right) & \dfrac{l_h}{I_p}\dfrac{\partial F_a}{\partial \Omega} \\ 0 & -l_h\dfrac{N_{gb}}{J_r}\left(\dfrac{\partial \tau_a}{\partial v} + k_\beta \dfrac{\partial \tau_a}{\partial \beta}\right) & \dfrac{N_{gb}}{J_r}\dfrac{\partial \tau_a}{\partial \Omega} \end{bmatrix} \tag{28}$$

This extra blade pitch in Eq. (26) is added to the collective blade pitch command from the PI controller, $K_{PI}(s)$ in Fig. 9, before the actuator saturation limits are applied. At first glance, it is observed that the extra feedback loop affects, not only the state transition from the platform pitch velocity to the generator speed, as shown by element $A^*(3,2)$ but also the damping of the platform pitch mode shown by element $A^*(2,2)$. This indicates that this parallel loop can be used for two control objectives: either to compensate for the RHPZs or to increase the platform pitch damping.

Solving for a gain that makes $A^*(3,2) = 0$ leads to full compensation of the effect of platform pitch on the generator speed. However, due to blade pitch coupling with both aerodynamic torque and thrust, such a gain reduces the effective system fore-aft damping as a side effect. It is, therefore, sensible to choose a smaller gain to partially compensate the fore-aft motion, which can be achieved by multiplying the parallel compensation gain by a static gain, ξ_β. The parallel compensation gain for blade pitch then becomes (Hegazy et al., 2023a; Stockhouse and Pao, 2024):

$$k_\beta = -\xi_\beta \frac{\partial \tau_a}{\partial v}\left(\frac{\partial \tau_a}{\partial \beta}\right)^{-1} \tag{29}$$

The value of $\xi_\beta \in [0,1]$ determines the degree of partial compensation from the blade pitch actuator to alleviate the effect of the platform pitch motion on the generator speed at the expense of less fore-aft damping. Should ~~this objective~~ the objective of decoupling the drivetrain and the platform dynamics be sought, extra filtering is required to change its dynamics~~, otherwise, it will be~~ ; otherwise, the system damping worsens and it becomes unstable. However, if the control objective shifts to increasing the fore-aft damping, that will be at the expense of reducing the drivetrain damping, thus resulting in less generator speed tracking performance. Similar to Eq. (13), the the platform pitch dynamics in the second row of $\boldsymbol{A}^*$ is represented in standard form as:

$$\delta\ddot{\theta} + \underbrace{\frac{1}{I_p}\left(C + l_h^2\frac{\partial F_a}{\partial v} + l_h k_\beta \frac{\partial F_a}{\partial \beta}\right)}_{2\zeta_p^*\omega_p}\delta\dot{\theta} + \underbrace{\frac{K}{I_p}}_{\omega_p^2}\delta\theta = 0, \tag{30}$$

where ζ_p^* is the new desired damping ratio of the platform pitch DoF, without any change in its natural frequency. According to Eq. (30) and taking Eq. (13) into account, k_β can be parametrised as (Stockhouse and Pao, 2024):

$$k_\beta = \frac{2\omega_p \Delta\zeta_p}{\frac{l_h}{I_p}\frac{\partial F_a}{\partial \beta}} = \frac{2\omega_p(\zeta_p^* - \zeta_p)}{\frac{l_h}{I_p}\frac{\partial F_a}{\partial \beta}}, \tag{31}$$

where $\Delta\zeta_p$ represents the desired change in the platform damping. The extra feedback loop acts as a damper, increasing the system damping by moving the poles of $G^*_{\Omega,\beta}$, corresponding to the platform pitch mode, away from their respective zeros. While the RHPZs remain unaffected, setting restrictions on the closed-loop control performance, which is evident from the phase loss of $180°$ in Fig. 10, the damper effect is illustrated, highlighting its direct influence on the outer loop $G^*_{\Omega,\beta}$. It is observed that the rotor dynamics deteriorate by adding the blade pitch damper as the depth of the anti-resonance dip increases, indicating an increase in generator speed oscillations, thereby affecting power production within the frequency range of the fore-aft mode.

Although the MIMO plant, $G(s)$ does not have any transmission zeros, the poor generator speed tracking performance is attributed to the persistence of the RHPZs in $G^*_{\Omega,\beta}$, as they are not affected by the parallel inner loop, and still impose a limitation on the PI controller bandwidth. This is confirmed by checking the numerator of $G^*_{\Omega,\beta}$, whose damping term becomes:

$$C + l_h^2\left(\underbrace{\frac{\partial F_a}{\partial v} - \frac{\partial \tau_a}{\partial v}\frac{\partial F_a}{\partial \beta}\left(\frac{\partial \tau_a}{\partial \beta}\right)^{-1}}_{\mu_{aero}} - \cancel{k_\beta l_h \frac{\partial F_a}{\partial \beta}} + \cancel{k_\beta l_h \frac{\partial F_a}{\partial \beta}}\right) \tag{32}$$

As shown in Eq. (32), the RHPZs are indeed unaffected since the inner-loop contribution cancels, thus leaving the RHPZs condition in Eq. (18) with no change.

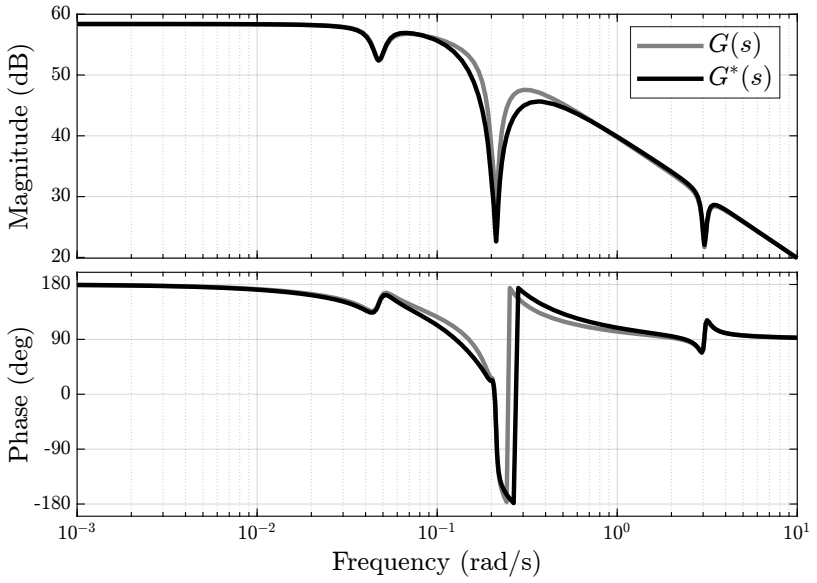

Figure 10. Bode plot comparing the channel mapping $\delta\beta$ to $\delta\Omega$ of the original transfer function $G(s)$ with the modified transfer function $G^*(s)$ depicted in Fig. 9, obtained after closing the inner loop from platform pitch velocity to blade pitch.

3.3.2 Parallel compensation: MIMO control structure

So far, the previous control strategies proved not to be able to compensate for the deteriorating effect of the RHPZs. The only way to move zeros is by parallel compensation, $y = (G + K)u$, which, if y is a physical output, can only be accomplished by adding an extra input (actuator) (Skogestad and Postlethwaite, 2005).

As mentioned earlier, the presence of zeros implies the blockage of certain input signals. In this case, the blade pitch input is blocked due to the emergence of RHPZs, which is depicted in Fig. 10 where anti-resonance dips exist, indicating a significant attenuation of the input signals at those frequencies. Therefore, instead of using the blade pitch in the parallel loop, the generator torque can be used as illustrated in Fig. 11, thus taking a step towards MIMO control. Unlike the blade pitch, the generator torque compensation is different as when $G_{\Omega,\beta}$, is closed with the generator torque parallel compensation loop, the RHPZs move to the LHP. At optimal gain, the RHPZs vanish from $G^*_{\Omega,\beta}$, which is the TF representing $G_{\Omega,\beta}$ after closing the generator torque parallel loop, indicating that the system became minimum phase. The generator torque parallel compensation uses proportional feedback of the platform pitch velocity (Fischer, 2013):

$$\delta\tau_g = -k_{\tau_g}\delta\dot{\theta} \tag{33}$$

Closing the inner feedback generator torque loop by substituting $\delta\tau_g$ from Eq. (33) in Eq. (3) and Eq. (12), the system matrix of the inner loop becomes:

$$\boldsymbol{A}^* = \begin{bmatrix} 0 & 1 & 0 \\ -\dfrac{K}{I_p} & -\dfrac{1}{I_p}\left(C + l_h^2 \dfrac{\partial F_a}{\partial v}\right) & \dfrac{l_h}{I_p}\dfrac{\partial F_a}{\partial \Omega} \\ 0 & \dfrac{N_{gb}}{J_r}\left(k_{\tau_g} N_{gb} - l_h \dfrac{\partial \tau_a}{\partial v}\right) & \dfrac{N_{gb}}{J_r}\dfrac{\partial \tau_a}{\partial \Omega} \end{bmatrix} \tag{34}$$

Therefore, to eliminate the effect of platform pitch rate on the rotor dynamics, set $\boldsymbol{A}^*(3,2) = 0$. Consequently, the parallel compensation gain for the generator torque actuator is (Fischer, 2013; Hegazy et al., 2023a; Stockhouse and Pao, 2024):

$$k_{\tau_g} = \xi_{\tau_g} \frac{l_h}{N_{gb}} \frac{\partial \tau_a}{\partial v}, \tag{35}$$

where $\xi_{\tau_g} \in [0,1]$ is introduced as a tunable parameter determining the intensity of parallel compensation since it is not necessary to remove the RHPZs totally. Having a glance at the numerator of $G^*_{\Omega,\beta}$, it can be noticed that adding the parallel compensation loop modifies the damping term in the numerator by modifying the aerodynamic coefficient, μ_{aero} in Eq. (18), to a new one, which in return, leads to a different zeros locations. The new aerodynamic coefficient becomes:

$$\tilde{\mu}_{aero} = \frac{\partial F_a}{\partial v} + (\xi_{\tau_g} - 1) \frac{\partial \tau_a}{\partial v} \frac{\partial F_a}{\partial \beta} \left(\frac{\partial \tau_a}{\partial \beta}\right)^{-1} \tag{36}$$

According to Eq. (36), the parallel compensation feedback loop makes it possible to manipulate the zeros of $G_{\Omega,\beta}$ and compensate for the RHPZs by pushing them towards the LHP ~~(Fischer, 2013; Yu et al., 2018; Hegazy et al., 2023a; Stockhouse et al., 2024b)~~ (Fischer, 2013; Yu et al., 2018; Hegazy et al., 2023a; Stockhouse et al., 2024b; Stockhouse and Pao, 2024). The level of compensation is tunable based on the tuning of the gain ξ_{τ_g}. The higher ξ_{τ_g}, the more the RHPZs move towards the LHP till they migrate to the LHP indicating the removal of those RHPZs. Consequently, the bandwidth of the PI controller can be increased above the platform pitch mode. This is clear in Fig. 12, as the depth of the anti-resonance dip, corresponding to the RHPZs, decreases meaning that the limitation set by the RHPZs is vanishing, which gives the opportunity to increase the aggressiveness of the PI controller.

The main drawback of this approach is the generator torque limit for parallel compensation that can be supplied by the actuator. The usage of the full-compensation gain ($\xi_{\tau_g} = 1$) eliminates the RHPZs, thus, turning the system to minimum phase for all operating points, however, the constraint imposed by the τ_g saturation restrains actuator signals exceeding the maximum generator torque. Reducing the compensation gain with $\xi_{\tau_g} \in [0,1]$ is rather advantageous in practice, as on one hand, it prohibits the generator torque actuator from saturating, and on the other hand, it reduces the drivetrain loads (Hegazy et al., 2023a). With $\xi_{\tau_g} < 1$, the RHPZs are partially compensated, allowing higher achievable bandwidth and, hence, improved performance.

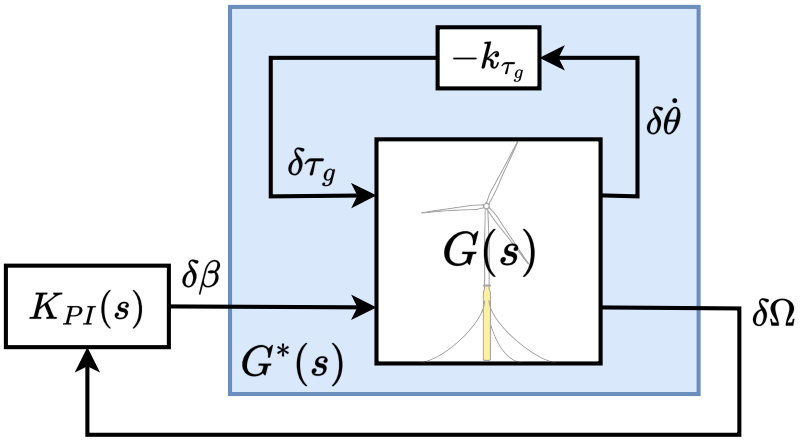

Figure 11. Block diagram of the generator torque parallel compensation (MIMO controller)

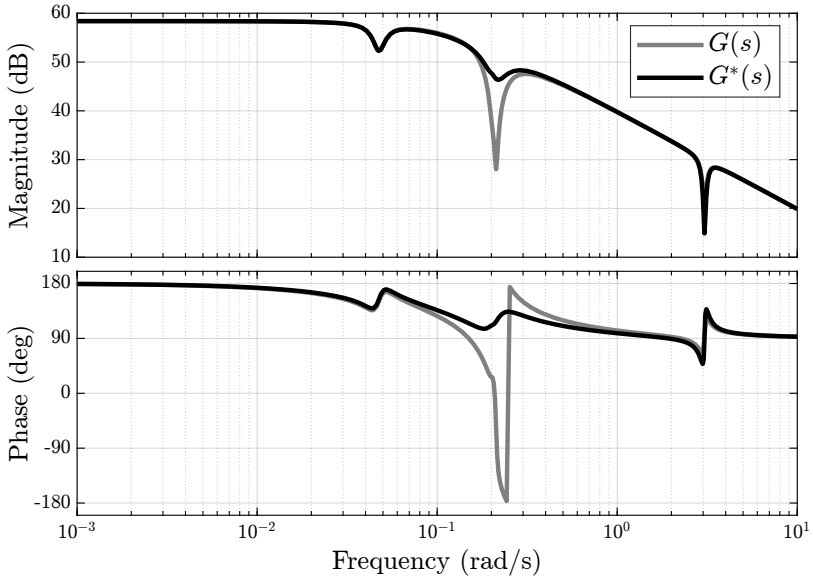

Figure 12. Bode plot comparing the original transfer function $G(s)$, which maps $\delta\beta$ to $\delta\Omega$, with the modified transfer function $G^*(s)$ depicted in Fig. 11, obtained after closing the parallel compensation feedback inner loop from platform pitch velocity to generator torque.

3.3.3 Parallel compensation: SIMO control structure

Hegazy et al. (2023a) showed that the feedback of the platform motion is not necessary for parallel compensation, as only generator speed can be used. They went on to show the control structure of the blade pitch and the generator torque controllers. It was learnt from $\mathcal{H}_\infty$ control synthesis that the blade pitch maintains the PI structure, while the generator torque requires ~~a band-pass filter.~~ an inverted-notch filter (Hegazy et al., 2023a). From its name, an inverted-notch filter is a control element that

is only operational at a specific frequency. Thinking about it, such a control structure, resulting from the $\mathcal{H}_\infty$ synthesis, for the generator torque control loop is reasonable since the generator torque input should not operate across all frequencies, but only around the RHPZs frequency where the blade pitch input is blocked. Therefore, the generator torque control loop takes over.

Figure 13 illustrates the control structure defined in Hegazy et al. (2023a), where the blade pitch controller maintains the PI control structure as:

$$K_\beta(s) = k_p + \frac{k_i}{s}, \tag{37}$$

where k_p and k_i are the proportional and the integral gains, respectively. As for the generator torque channel, an inverted notch is applied as:

$$K_{\tau_g}(s) = \frac{2\zeta_{\tau_g}\omega_{\tau_g}s}{s^2 + 2\zeta_{\tau_g}\omega_{\tau_g}s + \omega_{\tau_g}^2} \tag{38}$$

Consequently, the SIMO controller takes the form:

$$K(s) = \begin{bmatrix} K_{\tau_g}(s) \\ K_\beta(s) \end{bmatrix} \tag{39}$$

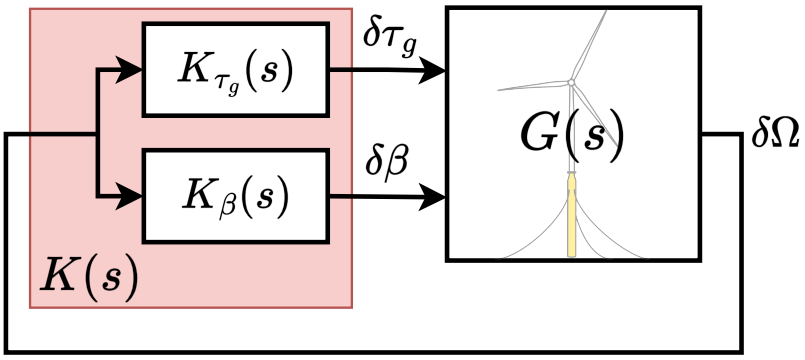

Figure 13. Block diagram of the FOWT closed-loop system, where $G(s)$ represents the plant model, and $K(s)$ represents the SIMO structure feedback controller composed of 2 SISO controllers; $K_{\tau_g}(s)$ controller acting on the generator torque actuator, and $K_\beta(s)$ active on the blade pitch actuator.

Now that the need for SIMO control to deal with the negative damping problem has been established in Fig. 13, tuning each controller separately sounds complicated due to the dynamic interactions between the MIMO channels that would arise when either of the controllers is modified. Therefore, the objective is to turn the SIMO system into a SISO one. In order to do that,

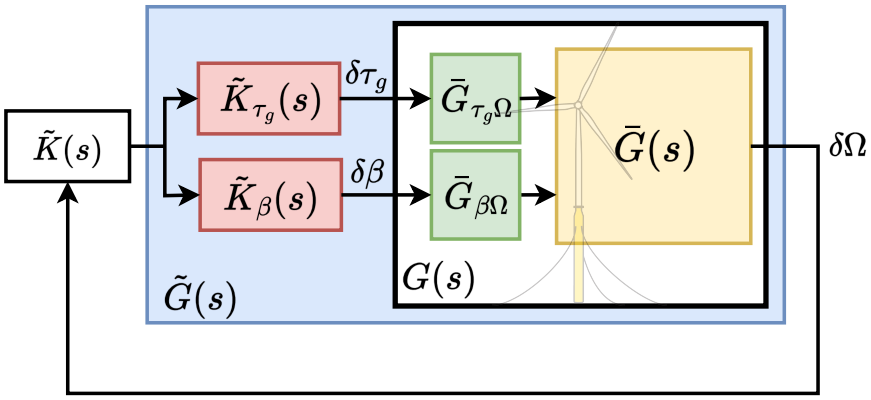

Figure 14. Transition from SIMO to SISO control structure

the original MISO plant $G(s)$ is normalised to $\bar{G}$ such that the magnitude of both the blade pitch and the generator torque input channels becomes unity so that both control inputs are of comparable effect. Afterwards, a linear combination of the two control elements $\bar{K}_{\tau_g}$ and $\bar{K}_{\beta}$ is combined with normalised MISO plant $\bar{G}$. This is depicted in Fig. 14 where the extra blocks are integrated with the plant such that there is a new plant ~~$G^*(s)$. This means that~~ $\tilde{G}(s)$. Therefore, the new SISO plant ~~$G^*(s)$~~ $\tilde{G}(s)$ is the result of the linear combination of both control channels as:

$$G^*\tilde{G}(s) = G\bar{G}(s)\tilde{K}(s)\begin{bmatrix}1\\1\end{bmatrix}, \tag{40}$$

~~In order to do that,~~ where the controllers $K_{\beta}(s)$ and $K_{\tau_g}(s)$ have to be decomposed such that:

$$K(s) = \begin{bmatrix}\tilde{K}_{\tau_g}(s)\\ \tilde{K}_{\beta}(s)\end{bmatrix}\tilde{K}(s) \tag{41}$$

where ~~a band-pass~~ an inverted notch filter is the outcome of combining a high-pass filter and an integrator:

$$K_{\tau_g}(s) = \tilde{K}(s)\tilde{K}_{\tau_g}(s) = \frac{2\zeta_{\tau_g}\omega_{\tau_g}\bar{k}}{s} \times \frac{s^2}{s^2 + 2\zeta_{\tau_g}\omega_{\tau_g}s + \omega_{\tau_g}^2}, \tag{42}$$

while a PI controller results from the combination of a PD and an integrator:

$$K_{\beta}(s) = \tilde{K}(s)\tilde{K}_{\beta}(s) = \frac{2\zeta_{\tau_g}\omega_{\tau_g}\bar{k}}{s} \times (\tilde{k}_p + \tilde{k}_d s), \tag{43}$$

where the PD controller gains are:

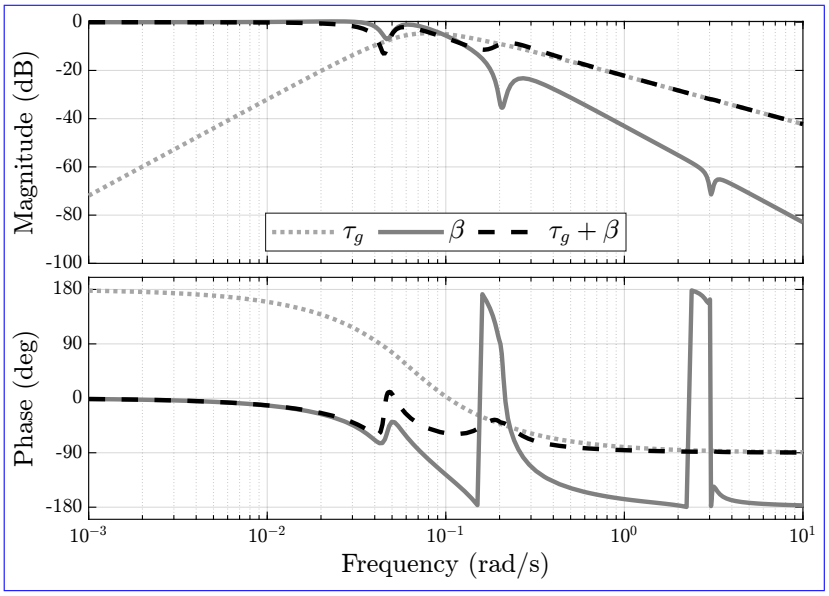

Figure 15. Bode plot of the normalised MISO plant $\bar{G}$ illustrating the ~~effect~~ frequency response of each control channel separately (solid lines) as well as the response of the SISO plant $\tilde{G}$ in case of the linear combination of both actuators (dashed line) where the blade pitch actuator is active till a certain frequency before its authority deteriorates, thus, the generator torque actuator takes over from that frequency onwards.

$$\tilde{k}_p = \frac{1}{2\zeta_{\tau_g}\omega_{\tau_g}} \tag{44}$$

$$\tilde{k}_d = \frac{1}{(2\zeta_{\tau_g}\omega_{\tau_g})^2} \tag{45}$$

In this work, the damping ratio of the inverted notch (ζ_{τ_g}) is set to 0.5, and its desired natural frequency ((ω_{τ_g})) is placed at the RHPZ location of $G_{\Omega,\beta}$. The gain $\bar{k}$ in $\tilde{K}(s)$ is a static gain to either crank up or reduce the overall gain of the controllers $\tilde{K}_{\tau_g}$ and $\tilde{K}_\beta$ simultaneously, and is kept at 1 in this paper. The objective is to tune one single controller instead of multiple control components, which would complicate the control tuning process.

The generator torque actuator is only active within the RHPZs frequency band to take over the control from the blade pitch, which is limited by the non-minimum phase behaviour around that band. This is depicted in Fig. 15, where the limitation set on the blade pitch, while regulating the generator speed, is lifted by the generator torque, and the linear combination of both actuators can lead to an increase in the control bandwidth, as shown in Fig. 16. The two vertical lines depict the closed-loop bandwidth of each controller. Clearly, the baseline feedback PI controller has its bandwidth constrained by the RHPZs, which are also around the platform pitch natural frequency. Looking at the loop transfer function of the linear combination of both

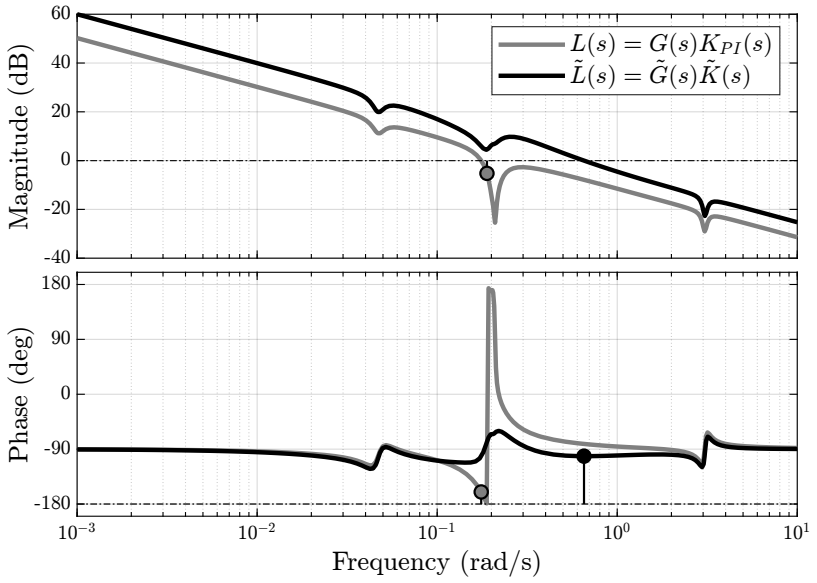

Figure 16. Bode plot of the loop transfer function, $L(s)$, of the baseline controller, $K_{PI}(s)$ and the SISO plant, $G(s)$ (grey), and the loop transfer of the artificial SISO plant, $\tilde{G}(s)$, in Fig. 14 and $\tilde{K}(s)$ illustrating the effect of the linear combination of both actuators on increasing the bandwidth of the closed-loop system indicated by the vertical lines in the phase plot.

actuators, we can see the jump in the bandwidth the SIMO controller makes over the baseline controller, as the SIMO controller intersects with the 0 dB line much later than the baseline controller. Moreover, the anti-resonance dip that corresponds to the RHPZs existing in the bode plot of the baseline controller is eliminated in the SIMO controller, reflecting on its robustness as it significantly increased with a phase margin of almost ~~90 deg~~90°.

4 Results

The FOWT system (NREL 5-MW RWT (Jonkman et al., 2009) atop OC3 floater (Jonkman, 2010)) was simulated in OpenFAST (NREL, 2025a) with the five controllers discussed in Section 3 in environmental conditions of turbulent wind and irregular waves. The simulations were conducted in the above-rated Region 3 ($v_{rated} = 11.4$ m/s) at average wind speeds ranging from 12 m/s to 24 m/s, with TurbSim (NREL, 2025b) to ~~generate~~ simulate the turbulent wind field, where the International Electrotechnical Commission (IEC) Kaimal spectral model was used as a turbulence model with a turbulence intensity of 14% and a wind shear exponent of 0.14. The irregular waves were generated using JONSWAP spectrum at a significant wave height $H_s = 3$ m and peak period $T_p = 12$ s. All the simulations were performed for a simulation time of 1200 s, with the first 600 s neglected for transients.

An example time-domain simulation at a reference wind speed of 18 m/s is illustrated in Figure 17 and Figure 18. The time traces are complemented with the power spectra for a detailed view of the controllers' performance. Looking at the rotor speed

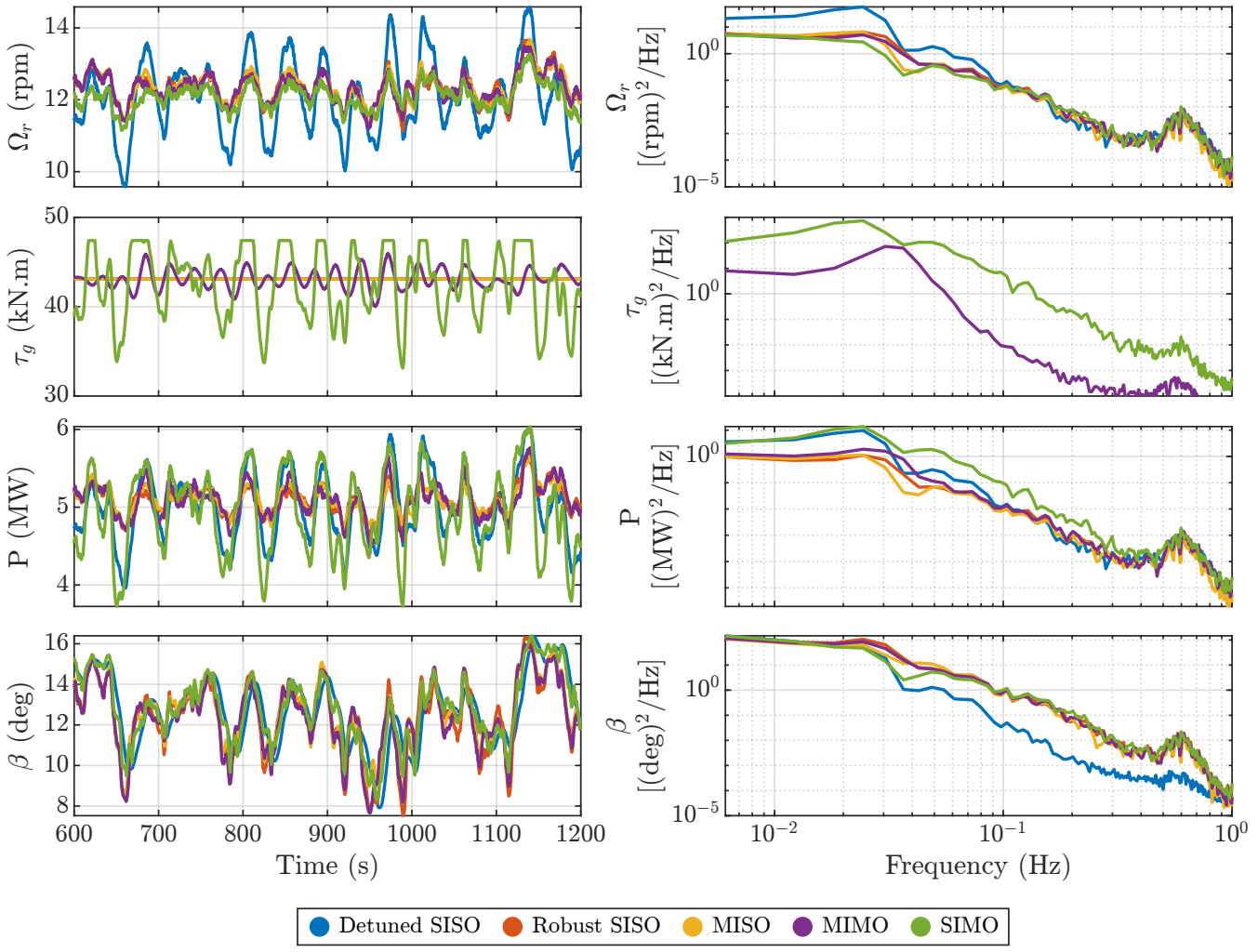

Figure 17. Non-linear simulation results for the FOWT system, simulated with each of the controllers described in Section 3 at a reference wind speed of 18 m/s.

signal in Figure 17, we can see the significant impact the robust tuning of the SISO PI controller can make in comparison to the detuned SISO PI controller. The rotor speed's peak-to-peak amplitude of the Robust SISO is significantly reduced compared to the detuned SISO. This is also evident in the spectral content of its power spectrum, as the rotor speed oscillations are suppressed till 0.1 Hz.

For the SISO controller, the generator torque is kept constant and the generator power in Region 3 is directly related to the generator speed. The reduction in the rotor speed oscillations reflects on the generator power leading to an improved power quality with less fluctuations. However, such an improved performance comes at the cost of actuation. This is to be expected

since the increased bandwidth of the Robust SISO means higher control activity, which can be seen in the blade pitch signal with higher spectral content across the frequency range, leading to an increase in the blade pitch variation.

Regarding the MISO controller in Fig. 17, its main objective is to add damping to the closed-loop system, through extra blade pitch action, to compensate for the severe reduction in the overall system damping caused by the negative aerodynamic damping as explained by Eqn. (18) and Eqn. (22). In this work, the MISO controller is composed of the Robust SISO controller, and added to it is the inner feedback loop from the platform pitch rate $\dot{\theta}$ to blade pitch as shown in Fig. 9. The MISO controller in Fig. 17 appears to be doing slightly better than the Robust SISO in a small frequency segment within the low-frequency region before 0.05 Hz, while no significant difference is observed between both controllers at other frequencies. Similar to the detuned and Robust SISO cases, the generator power follows the same trend as the rotor speed since the generator torque is constant in the case of the MISO controller. This explains the absence of the generator torque curves relevant to the three cases in the power spectrum. The MISO controller blade pitch actuation does not change much from the Robust SISO controller. It simply is a bit more active and thus more oscillatory because of the extra blade pitch input added.

As for the MIMO controller in Fig. 17, the generator torque is employed as an extra actuator to provide parallel compensation (Skogestad and Postlethwaite, 2005) to the FOWT system to deal with the RHPZs. Implementing the MIMO controller results in a modest enhancement of rotor speed, as the substantial improvement achieved by the Robust SISO controller over the detuned version significantly limits the potential for further error reduction. With the generator torque not constant anymore, the power variation includes contributions from both generator speed and generator torque, showing a clear drawback of the MIMO controller.

Transitioning to the newly proposed control structure, the SIMO controller demonstrates superior performance in generator speed regulation—the primary objective of this controller—particularly when compared to the Detuned SISO controller. While one might expect increased blade pitch activity to achieve better generator speed regulation, this is not the case. Instead, the blade pitch action remains nearly identical to that of the Robust SISO, MISO, and MIMO controllers. This is because, beyond a certain point, generator torque takes over, as previously shown in Fig. 15. Consequently, the generator torque response becomes highly aggressive, exhibiting significant variations to maintain a more stable generator speed signal, even reaching saturation. However, this comes at the expense of power quality, similar to the MIMO controller. Notably, the SIMO controller exhibits an even more aggressive generator torque action than the MIMO controller. A less aggressive tuning of the SIMO controller would reduce the actuator usage and improve the power quality. Nevertheless, if the power quality is the main control objective, a controller aimed at that objective could be synthesised, but at the cost of increased drivetrain loads (Stockhouse and Pao, 2024).

Across the above-rated wind speed spectrum, the SIMO controller achieves the lowest rotor speed oscillations, as indicated by the standard deviation, without any notable difference in blade pitch action compared to other controllers (see Fig. 19). However, the generator torque experiences a large increase with the SIMO controller, even at wind speeds where the RHPZs are expected to disappear (above 16 m/s). This is because, unlike other controllers, the SIMO controller continuously engages the generator torque actuator across all wind speeds, including those without RHPZs. As a result, variations in generator speed have a considerable impact on generator power. In the simulations conducted at reference wind speeds of 12–14 m/s, the system occasionally operates below the rated wind speed, leading to fluctuations in generator torque. This occurs despite the

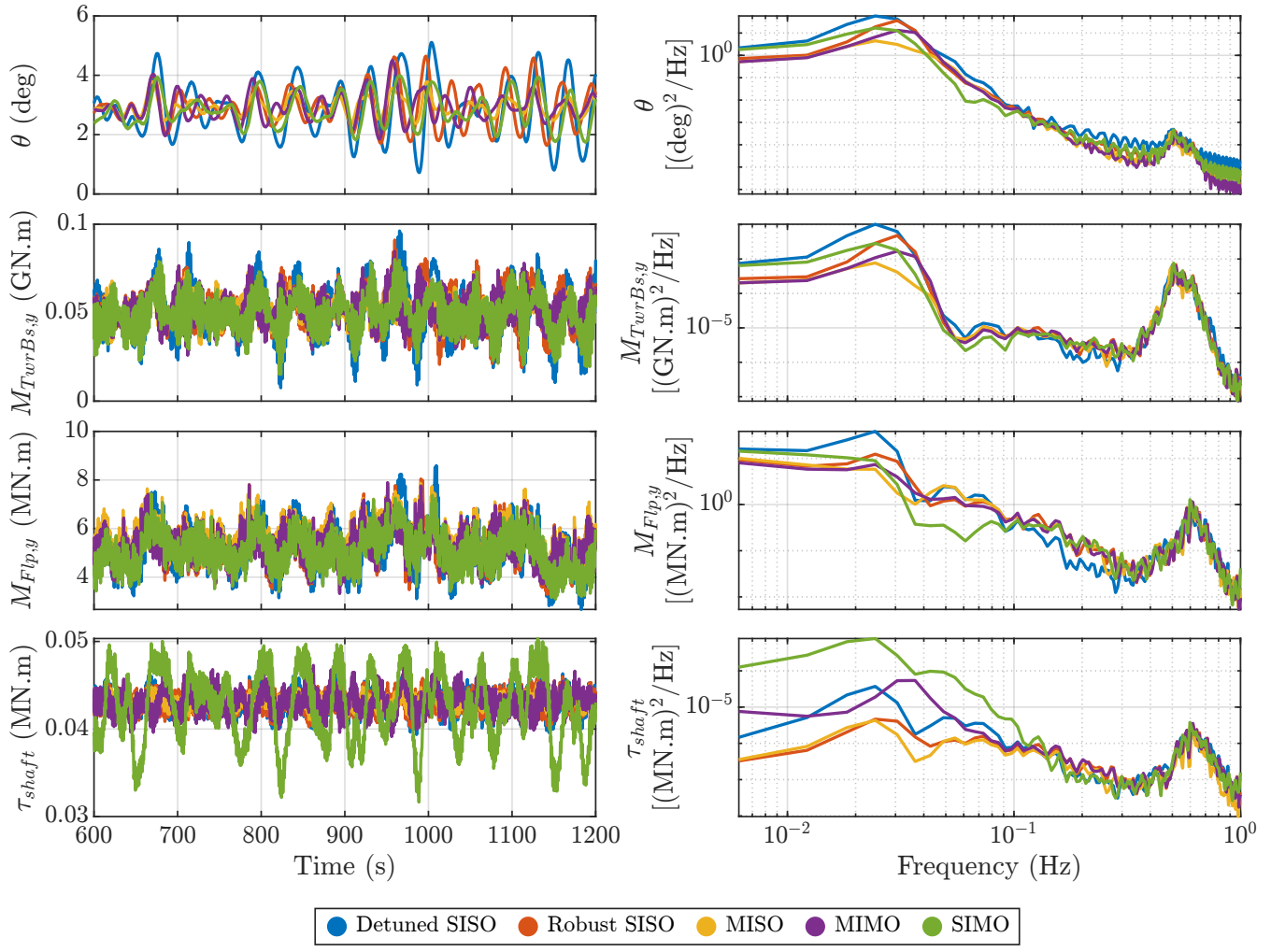

Figure 18. Non-linear simulation results for the FOWT system, simulated with each of the controllers described in Section 3 at a reference wind speed of 18 m/s.

Detuned SISO, Robust SISO, and MIMO controllers being designed to maintain a constant generator torque with zero standard deviation in Region 3—a condition that is fully realised at wind speeds above 14 m/s.

Examining Fig. 18 and Fig. 19 simultaneously, it is evident that all controllers reduce platform pitch oscillations compared to the fluctuations observed with the Detuned SISO. Among them, the MISO controller achieves the greatest reduction, as it is specifically designed to enhance platform pitch damping—an effect clearly visible in the power spectrum around the platform pitch eigenfrequency (≈ 0.033 Hz).

Although the SIMO controller is primarily designed to mitigate generator speed fluctuations, it also succeeds in reducing platform pitch oscillations below the Detuned SISO level. While its effectiveness in this regard is lower than that of the MISO and MIMO controllers, this reduction remains beneficial.

Furthermore, this improvement extends to the tower base fore-aft moment ($M_{TwrBs,y}$), as there is a strong correlation between platform pitch motion and tower base loading. Consequently, controllers that effectively suppress platform oscillations also contribute to significant tower fatigue reduction.

Regarding the blade-root flapwise moment ($M_{Flp,y}$), all controllers outperform the Detuned SISO across all wind speeds, as shown in Fig. 19. This improvement is evident at low frequencies up to 0.1 Hz, after which there is a slight drop in performance, temporarily exceeding the level of the Detuned SISO. Beyond this point, all controllers converge, exhibiting no significant differences, as depicted in Fig. 18.

Rotor-shaft torsional loading (τ_{shaft}) is a well-known drawback of torque feedback in wind turbine control systems. While both the Robust SISO and MISO controllers exhibit smaller shaft loading excursions compared to the Detuned SISO, the MIMO and SIMO controllers, which rely on torque feedback, introduce greater fluctuations in shaft torsional loading. As shown in Fig. 18, this effect is particularly pronounced in the SIMO controller, which exhibits elevated shaft loading variations across all wind speeds, as further illustrated in Fig. 19.

Based on these findings, the authors recommend an adaptive approach, where different proposed controllers are alternated depending on environmental conditions and control objectives. For example, at certain times, the turbine operator may prioritise minimising generator speed oscillations and activate the corresponding controller. At other times, the focus may shift to reducing structural loading, necessitating a different control strategy. Since no single controller can simultaneously optimise all objectives—some of which may be conflicting—dynamic selection based on operational priorities is advised.

Another recommendation is to incorporate a feedforward control strategy to reduce dependence on reactive feedback control. If an accurate preview of disturbances affecting the FOWT is available, a LiDAR feedforward controller (Schlipf et al., 2020) targeting the wind turbulence and a wave feedforward controller (Hegazy et al., 2023b, 2024) targeting the wave forces can be implemented to mitigate the effects of wind and wave disturbances on the FOWT, respectively. This approach alleviates the need for a high-bandwidth feedback controller, as the feedforward controllers would handle most of the disturbance rejection.

5 Conclusion

A new fixed-structure controller has been developed for FOWTs to effectively mitigate the well-known "negative damping" instability and address the non-minimum phase behaviour introduced by the persistent RHPZs in $G_{\Omega\beta}$. Designed specifically for generator speed regulation, the proposed controller was evaluated through non-linear simulations in OpenFAST, where it outperformed the existing FOWT controllers from the literature. Furthermore, it demonstrated robustness in a high-fidelity simulation environment, effectively handling additional system dynamics.

The primary advantage of the proposed FOWT controller is that it operates without requiring any additional sensors, preserving the conventional SISO configuration by relying exclusively on generator speed measurement. This approach enhances

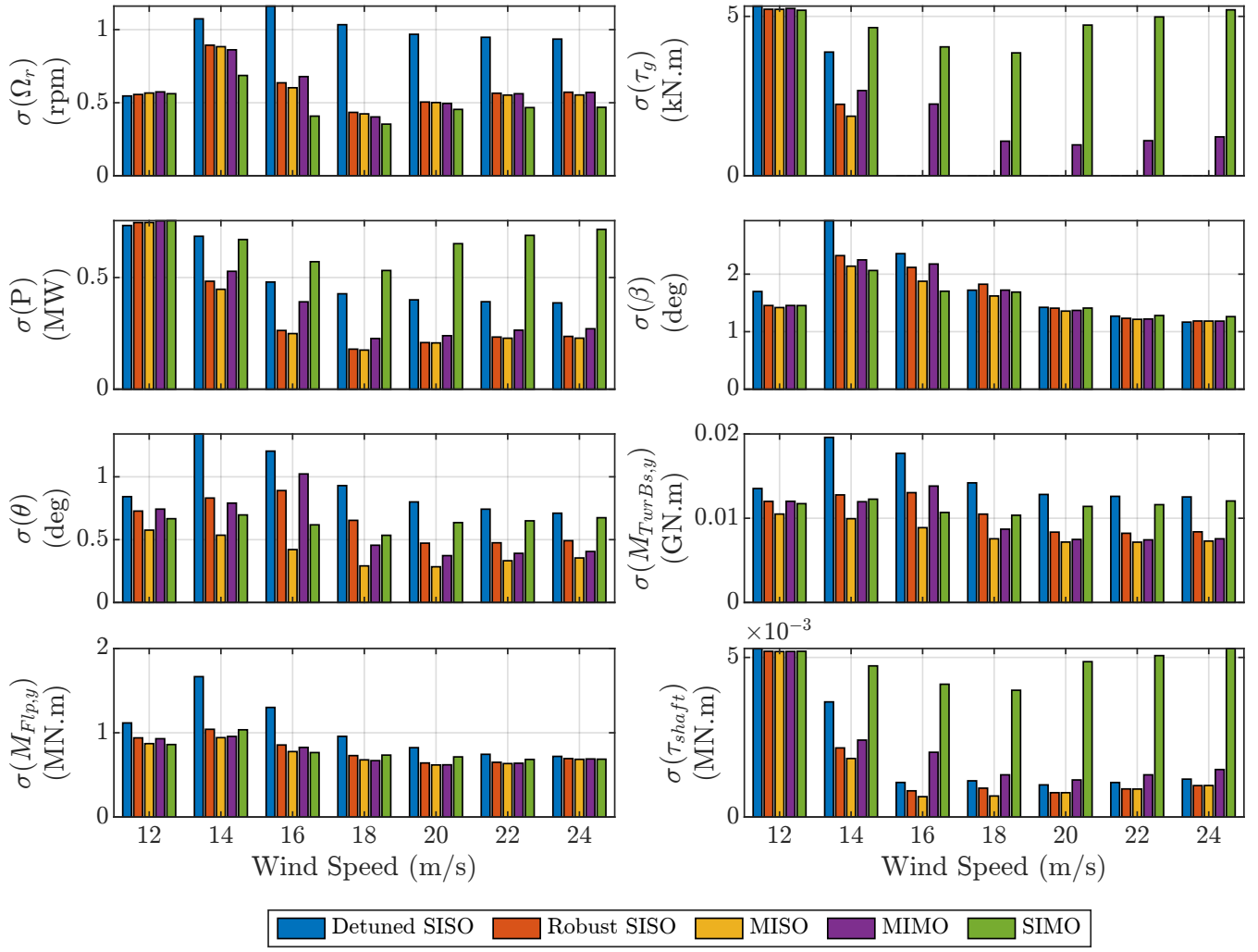

Figure 19. Controller performance: Non-linear simulation results for the FOWT, simulated with each of the controllers described in Section 3 at a reference wind speed of 18 m/s.

robustness, as incorporating extra signals can increase sensitivity to unmodeled dynamics. Additionally, the controller can be regarded as an artificial SISO controller, as shown in Fig. 14 and Fig. 15, where the plant transfer function is pre-filtered to achieve the desired control performance.

While the MIMO controller features a simpler control structure compared to the SIMO controller, the SIMO configuration provides built-in redundancy within the FOWT system, ensuring continued operation in the event of floating platform sensor failure. If the wind turbine is equipped with platform pitch sensors and the MIMO controller is in use, a sensor malfunction could compromise performance. In such a scenario, the SIMO controller acts as a backup solution, allowing the system to operate despite the loss of platform pitch measurements.

Incorporating inner loops into the standard control loop $G_{\Omega,\beta}$, whether using MISO, SIMO, or MIMO structures, expands the design space for the SISO PI feedback controller, enabling the achievement of higher bandwidth. However, a well-known drawback of employing generator torque actuation for parallel compensation is the resulting increase in shaft and drivetrain loads (Fischer, 2013), along with deteriorated power quality. To mitigate power quality concerns, alternative MIMO feedback architectures, such as a constant-power controller (Stockhouse and Pao, 2024), can be integrated.

Furthermore, the cost function in the robust control tuning approach from Stockhouse and Pao (2024) has been modified to prevent actuator saturation. Without this adjustment, actuator activity could become unbounded, leading to simulation ~~failure~~instability. This refinement has enhanced performance in the primary objectives of generator speed regulation and tower load reduction, even in the presence of modelling inaccuracies resulting from dynamic simplifications and omitted degrees of freedom.

Code and data availability. The code and data presented in this work can be made available upon request.

Author contributions. AH conceptualisation, methodology, investigation, writing – original daft under the super-vision of PN and JWVW. The insights and conclusion presented in this paper are the results of extensive discussions among the co-authors. All co-authors thoroughly reviewed the article.

Competing interests. At least one of the (co-)authors is a member of the editorial board of Wind Energy Science. The peer-review process was guided by an independent editor, and the authors also have no other competing interests to declare.

Acknowledgements. This project is part of the FLOATFARM project. The research presented in this paper has received funding from the European Union's Horizon 2020 research and innovation programme under grant agreement no. 101136091.

References

Robust gain scheduling baseline controller for floating offshore wind turbines, 23.

Abbas, N. J., Zalkind, D. S., Pao, L., and Wright, A.: A reference open-source controller for fixed and floating offshore wind turbines, Wind Energy Science, 7, 53–73, 2022.

Åström, K. J. and Murray, R. M.: Feedback systems: an introduction for scientists and engineers, Princeton university press, 2021.

Bossanyi, E. A.: The design of closed loop controllers for wind turbines, Wind energy, 3, 149–163, https://doi.org/https://doi.org/10.1002/we.34, 2000.

Brandetti, L., Mulders, S. P., Liu, Y., Watson, S., and van Wingerden, J.-W.: Analysis and multi-objective optimisation of wind turbine torque control strategies, Wind Energy Science, 8, 1553–1573, https://doi.org/10.5194/wes-8-1553-2023, 2023.

Burton, T., Jenkins, N., Sharpe, D., and Bossanyi, E.: Wind energy handbook, John Wiley & Sons, 2021.

Cummins, W.: The impulse response function and ship motion, Tech. rep., 1961.

De Corcuera, A. D., Pujana-Arrese, A., Ezquerra, J. M., Segurola, E., and Landaluze, J.: H∞ Based Control for Load Mitigation in Wind Turbines, Energies, 5, 938–967, https://doi.org/10.3390/en5040938, 2012.

Doyle, J. C., Francis, B. A., and Tannenbaum, A. R.: Feedback control theory, Courier Corporation, 2013.

European Commission: European Wind Power Action Plan., https://energy.ec.europa.eu/system/files/2023-10/COM_2023_669_1_EN_ACT_part1_v8.pdf, (accessed: 16-11-2023), 2023.

Fischer, B.: Reducing rotor speed variations of floating wind turbines by compensation of non-minimum phase zeros, 7, 413–419, https://doi.org/10.1049/iet-rpg.2012.0263, 2013.

Fischer, B. and Loepelmann, P.: Balancing rotor speed regulation and drive train loads of floating wind turbines, in: Journal of Physics: Conference Series, vol. 753, p. 052016, IOP Publishing, 2016.

Fleming, P., Wingerden, J.-W., and Wright, A.: Comparing State-Space Multivariable Controls to Multi-SISO Controls for Load Reduction of Drivetrain-Coupled Modes on Wind Turbines through Field-Testing, https://doi.org/10.2514/6.2012-1152, 2012.

Fleming, P. A., Pineda, I., Rossetti, M., Wright, A. D., and Arora, D.: Evaluating methods for control of an offshore floating turbine, in: International Conference on Offshore Mechanics and Arctic Engineering, vol. 45547, p. V09BT09A019, American Society of Mechanical Engineers, 2014.

Fontanella, A., Al, M., Van Der Hoek, D., Liu, Y., Van Wingerden, J. W., and Belloli, M.: A control-oriented wave-excited linear model for offshore floating wind turbines, Journal of Physics: Conference Series, 1618, https://doi.org/10.1088/1742-6596/1618/2/022038, 2020.

GWEC: Global Wind Report 2025, Tech. rep., Global Wind Energy Council, 2025.

Hegazy, A., Naaijen, P., and van Wingerden, J. W.: A novel control architecture for floating offshore wind turbines, in: IFAC 22nd World Congress, 2023a.

Hegazy, A., Naaijen, P., and van Wingerden, J.-W.: Wave Feedforward Control for Large Floating Wind Turbines, in: 2023 IEEE Conference on Control Technology and Applications (CCTA), pp. 593–598, IEEE, 2023b.

Hegazy, A., Naaijen, P., Leroy, V., Bonnefoy, F., Mojallizadeh, M. R., Pérignon, Y., and van Wingerden, J.-W.: The potential of wave feedforward control for floating wind turbines: a wave tank experiment, Wind Energy Science, 9, 1669–1688, https://doi.org/10.5194/wes-9-1669-2024, 2024.

Jonkman, J.: Influence of Control on the Pitch Damping of a Floating Wind Turbine, in: 46th AIAA Aerospace Sciences Meeting and Exhibit, American Institute of Aeronautics and Astronautics, https://doi.org/10.2514/6.2008-1306, 2008.

Jonkman, J.: Definition of the Floating System for Phase IV of OC3, Tech. rep., National Renewable Energy Lab.(NREL), Golden, CO (United States), 2010.

Jonkman, J., Butterfield, S., Musial, W., and Scott, G.: Definition of a 5-MW Reference Wind Turbine for Offshore System Development, https://doi.org/10.2172/947422, 2009.

Larsen, T. J. and Hanson, T. D.: A method to avoid negative damped low frequent tower vibrations for a floating, pitch controlled wind turbine, 75, 012 073, https://doi.org/10.1088/1742-6596/75/1/012073, 2007.

Leithead, W. E. and Dominguez, S.: Coordinated Control Design for Wind Turbine Control Systems, 2006.

Lemmer, F., Schlipf, D., and Cheng, P. W.: Control design methods for floating wind turbines for optimal disturbance rejection, in: Journal of Physics: Conference Series, vol. 753, p. 092006, IOP Publishing, 2016.

Lemmer, F., Yu, W., Schlipf, D., and Cheng, P. W.: Robust gain scheduling baseline controller for floating offshore wind turbines, 23, 17–30, https://doi.org/10.1002/we.2408, 2020.

Lukovic, M. K., Tian, Y., and Matusik, W.: Diversity-Guided Multi-Objective Bayesian Optimization With Batch Evaluations, in: Advances in Neural Information Processing Systems, edited by Larochelle, H., Ranzato, M., Hadsell, R., Balcan, M., and Lin, H., vol. 33, pp. 17 708–17 720, Curran Associates, Inc., https://proceedings.neurips.cc/paper_files/paper/2020/file/cd3109c63bf4323e6b987a5923becb96-Paper.pdf, 2020.

Namik, H., Stol, K., and Jonkman, J.: State-space control of tower motion for deepwater floating offshore wind turbines, in: 46th AIAA aerospace sciences meeting and exhibit, p. 1307, https://doi.org/10.2514/6.2008-1307, 2008.

Nielsen, F. G., Hanson, T. D., and Skaare, B.: Integrated Dynamic Analysis of Floating Offshore Wind Turbines, pp. 671–679, ASMEDC, https://doi.org/10.1115/OMAE2006-92291, 2006.

NREL: National Renewable Energy Laboratory, OpenFAST, https://www.nrel.gov/wind/nwtc/openfast.html, 2025a.

NREL: National Renewable Energy Laboratory, TurbSim, https://www.nrel.gov/wind/nwtc/turbsim.html, 2025b.

Pao, L. Y., Pusch, M., and Zalkind, D. S.: Control Co-Design of Wind Turbines, Annual Review of Control, Robotics, and Autonomous Systems, 7, 201–226, https://doi.org/https://doi.org/10.1146/annurev-control-061423-101708, 2024.

Perez, T. and Fossen, T. I.: A matlab toolbox for parametric identification of radiation-force models of ships and offshore structures, https://doi.org/10.4173/mic.2009.1.1, 2009.

Saenz-Aguirre, A., Ulazia, A., Ibarra-Berastegi, G., and Saenz, J.: Floating wind turbine energy and fatigue loads estimation according to climate period scaled wind and waves, Energy Conversion and Management, 271, 116 303, 2022.

Schlipf, D., Lemmer, F., and Raach, S.: Multi-variable feedforward control for floating wind turbines using lidar, in: ISOPE International Ocean and Polar Engineering Conference, pp. ISOPE–I, ISOPE, 2020.

Skogestad, S. and Postlethwaite, I.: Multivariable feedback control: analysis and design, john Wiley & sons, 2005.

Stockhouse, D. and Pao, L. Y.: Multiloop Control of Floating Wind Turbines: Tradeoffs in performance and stability, IEEE Control Systems, 44, 63–80, https://doi.org/10.1109/MCS.2024.3432340, 2024.

Stockhouse, D., Phadnis, M., Henry, A., Abbas, N. J., Sinner, M., Pusch, M., and Pao, L. Y.: A Tutorial on the Control of Floating Offshore Wind Turbines: Stability Challenges and Opportunities for Power Capture, IEEE Control Systems, 44, 28–57, https://doi.org/10.1109/MCS.2024.3433208, 2024a.

Stockhouse, D., Pusch, M., Damiani, R., Sirnivas, S., and Pao, L.: Robust multi-loop control of a floating wind turbine, Wind Energy, 27, 1205–1228, https://doi.org/https://doi.org/10.1002/we.2864, 2024b.

van der Veen, G. J., Couchman, I. J., and Bowyer, R.: Control of floating wind turbines, in: 2012 American Control Conference (ACC), pp. 3148–3153, IEEE, https://doi.org/10.1109/ACC.2012.6315120, 2012.

WindEurope: Wind energy in Europe: 2024 Statistics and the outlook for 2025-2030, 2025.

Yu, W., Lemmer, F., Schlipf, D., Cheng, P. W., Visser, B., Links, H., Gupta, N., Dankemann, S., Counago, B., and Serna, J.: Evaluation of control methods for floating offshore wind turbines, Journal of Physics: Conference Series, 1104, 012 033, https://doi.org/10.1088/1742-6596/1104/1/012033, 2018.

Yu, W., Lemmer, F., Schlipf, D., and Cheng, P. W.: Loop shaping based robust control for floating offshore wind turbines, in: Journal of Physics: Conference Series, vol. 1618, p. 022066, IOP Publishing, 2020.